DR. SARAH PERRY FLANAGAN (Orcid ID : 0000-0002-2226-4213)

The population genomics of repeated freshwater colonizations by Gulf pipefish

Sarah P. Flanagan[1]*, Emily Rose[2], and Adam G. Jones[3]

[1] School of Biological Sciences, University of Canterbury, 4800 Private Bag, Christchurch 8140, New Zealand

[2] Department of Biology, Valdosta State University, Valdosta, GA, 31698

[3] Department of Biological Sciences, University of Idaho, Moscow, ID 83844

*Corresponding Author, Email: spflanagan.phd@gmail.com, Phone: +64 3 36 90433

Running head: Population genomics of freshwater colonization

Abstract

How organisms adapt to the novel challenges imposed by the colonization of a new habitat has long been a central question in evolutionary biology. When multiple populations of the same species independently adapt to similar environmental challenges, the question becomes whether the populations have arrived at their adaptations through the same genetic mechanisms. In recent years, genetic techniques have been used to tackle these questions by investigating the genome-level changes underlying local adaptation. Here, we present a genomic analysis of colonization of freshwater habitats by a primarily marine fish, the Gulf pipefish (*Syngnathus scovelli*). We sample pipefish from four geographically distinct freshwater locations and use double-digest restriction site associated DNA sequencing to compare them to twelve previously studied saltwater populations. The two most geographically distant and isolated freshwater populations are the most genetically distinct, although demographic analysis suggests that these populations experience ongoing migration with their saltwater neighbors. Additionally, outlier regions were found genome-wide, showing parallelism across ecotype pairs. We conclude that these multiple freshwater colonizations involve similar genomic regions, despite the large geographic distances and different underlying mechanisms. These similar patterns are likely facilitated by the interacting effects of intrinsic barriers, gene flow among populations, and ecological selection in the Gulf pipefish.

Introduction

An important goal of evolutionary biology is to understand how species cope with new selective pressures, a topic with implications for speciation (Schluter & Conte, 2009), development (Laugen, Laurila, Räsänen, & Merilä, 2003), disease (Sternberg & Thomas, 2014), and conservation (Hoffmann & Sgro, 2011). When populations are geographically isolated for long periods of time, new mutations accumulate in different regions and local selection pressures can act on those alleles (Le Moan, Gagnaire, & Bonhomme, 2016; Portik et al., 2017; Rougemont & Bernatchez, 2018; Rougeux, Bernatchez, & Gagnaire, 2017; Tine et al., 2014). However, ecological divergence can also occur in sympatry and over relatively rapid timescales, with examples of divergence occurring despite ongoing gene flow with source populations (Junge et al., 2011) and admixture with local populations or species (Ravinet et al., 2015; Riquet et al., 2019; Westram et al., 2018). These two paradigms for understanding speciation are at the heart of long-standing controversies in speciation research (Mayr, 1947; Via, 2001; White, 1968), but investigating the mechanisms underlying ongoing divergence among populations can allow for further insight into the speciation process.

In some cases, when multiple populations have colonized similar environments and converged on similar ecotypes (i.e., parallel evolution), understanding the origin of locally adaptive alleles becomes critical to compare the mechanisms linking populations and shed light on the repeatability of evolution (Elmer & Meyer, 2011; Nosil et al., 2018; Schluter & Conte, 2009). Sympatric speciation models allow for the sharing of locally adapted alleles either through ongoing migration or through ancestral gene flow (e.g., Schield et al., 2018). This important role for historical processes (i.e., shared evolutionary histories) has been highlighted by recent examples from reef fishes (DiBattista et al., 2020), threespine sticklebacks (Rennison, Delmore, Samuk, Owens, & Miller, 2020), and lamprey (Xue & Hickerson, 2020). Alternatively, in allopatric models, locally adaptive mutations could have arisen *de novo* in each population, allowing phenotypes to converge through the same mutations, (Hill et al., 2019), similar mutations (Gallant et al., 2014; Kratochwil et al., 2018; Soria-Carrasco et al., 2014), or through different mutations (Stern, 2013; Tenaillon et al., 2012). When populations are isolated for a period of time but then come into secondary contact, novel alleles are expected to arise and then be exchanged (Gompert, Lucas, Fordyce, Forister, & Nice, 2010). A variant of this secondary contact model is the transporter hypothesis (Schluter & Conte, 2009), in which a locally

adaptive allele arises in an initial population, spreads back to the source population through gene flow, and ultimately rises in frequency in each population segment that subsequently encounters the novel environment (Butlin et al., 2014; Schluter & Conte, 2009).

One challenge in differentiating between these alternative scenarios is that genetic barriers to gene flow are not homogeneously distributed throughout the genome, and a single genomic region may not accurately reflect the scenarios of population-level isolation and migration (Ravinet et al., 2017). When populations have diverged for long periods of time, genetic incompatibilities can accumulate at some loci, resulting in reduced effective migration rates at given genomic regions, or 'barrier loci' (Wu, 2001). However, barrier loci can also be created by divergent selection due to the differing environments despite ongoing gene flow, as can other barriers to gene flow such as assortative mate choice or postzygotic isolation (Ravinet et al., 2017; Wu, 2001). These barrier loci have been shown to play an important role in ecological speciation, such as in the adaptation to freshwater by lampreys (Rougemont et al., 2017). Additionally, loci experience a reduced effective population size, N_e, due to linked selection (Cruickshank & Hahn, 2014; Ravinet et al., 2017), which can also contribute to population differentiation (e.g., Rougeux et al., 2017). When multiple mechanisms coincide, their impact on reducing gene flow at a locus can be amplified, though differentiating between barrier effects can become challenging (Barton, 1979; Bierne, Welch, Loire, Bonhomme, & David, 2011; Butlin & Smadja, 2018). Therefore, it is critical to incorporate heterogeneous rates of migration and effective population size when testing hypotheses about the demographic histories and barriers to gene flow contributing to ecological speciation (Roux et al., 2014, 2016), for instance by comparing the fit of a variety of evolutionary models to the observed site-frequency spectrum or population divergence statistics, using diffusion approximation (Gutenkunst, Hernandez, Williamson, & Bustamante, 2009; Portik et al., 2017) or approximate Bayesian computation models (Excoffier, Hofer, & Foll, 2009; Roux et al., 2016; Xue & Hickerson, 2020).

We encountered a unique opportunity to test hypotheses about ecological speciation in a species with limited dispersal (Bertola et al., 2020), the Gulf pipefish (*Syngnathus scovelli*). During the course of a previous study (Flanagan, Rose, & Jones, 2016), which identified patterns of isolation-by-distance in 12 marine populations of *S. scovelli*, we encountered four geographically distinct

freshwater populations. These four populations were found in separate lakes or bays in four different states (Texas, Louisiana, Alabama, and Florida; Fig. 1). The dates of freshwater colonization are unknown, but breeding populations of Gulf pipefish were documented in the Florida and Louisiana freshwater sites in the 1940s (McLane, 1955) and 1960s (Whatley, 1962, 1969), respectively. The Texas freshwater site, Lake Texana, is a landlocked reservoir, and Gulf pipefish were first described as breeding there in 2011 (Martin, Cohen, Labay, Casarez, & Hendrickson, 2013). Although secondary introduction is possible, Martin et al. (2013) hypothesized that the pipefish were living in the Navidad River, which feeds the reservoir, when the dam was constructed in 1981. As for the Alabama site, a previous population genetics study using microsatellite loci identified significant population structure between marine and freshwater populations of *S. scovelli* in Alabama (Partridge, Boettcher, & Jones, 2012).

Pipefish have some biological traits that are relevant to their ability to adapt to freshwater environments. Gulf pipefish are a polyandrous, sex-role-reversed species with male pregnancy (Jones & Avise, 1997), and females experience strong sexual selection (Flanagan, Johnson, Rose, & Jones, 2014; Jones, Walker, & Avise, 2001; Rose, Paczolt, & Jones, 2013). Gulf pipefish have more limited dispersal than other marine organisms due to male pregnancy, a preference for near-shore habitats, and a low propensity for dispersal via rafting (Bertola et al., 2020). This limited dispersal is likely to promote population differentiation by reducing gene flow (Lenormand, 2002), an expectation that is reflected in our previous results showing isolation by distance driving genomic patterns in marine populations (Flanagan et al., 2016). Pregnant male *S. scovelli* regulate the osmotic environment their embryos experience, particularly in the early stages of development before embryos have developed osmoregulatory organs (Partridge, Shardo, & Boettcher, 2007; Quast & Howe, 1980). Osmotic regulation is one of the major challenges facing organisms that transition between marine and freshwater environments (Potts & Hedges, 1991). In pregnant male pipefish, osmotic regulation is likely mediated by numerous chloride cells in their brood pouches, which show structural resemblance to gill tissues in the closely related species *Syngnathus abaster* and *S. acusimilis* (Carcupino, 2002; Serkov, Kornienko, & Kolobov, 2007). Syngnathids also have aglomerular kidneys with an abundance of Na-K-ATPase pumps, which means that they must use additional mechanisms such as NaCl retention and secretion to maintain a homeostatic state (Fogelson et al., 2015). These

osmotic characteristics, combined with the likelihood for geographically distant populations to diverge, indicate that pipefish populations might readily adapt to freshwater habitats.

Here, we use a population genomics approach to investigate whether four distinct freshwater populations represent independent colonizations of freshwater habitats, and whether they are genetically distinct from marine populations. We further assess whether these populations use novel molecular adaptations or shared variation in repeated freshwater colonizations by *S. scovelli* and investigate the genomic basis of local adaptation to freshwater.

Methods

Sample collection

This study involved a total of 16 Gulf pipefish collection sites, including 12 marine sites and four freshwater sites. The population genomics of the marine populations, which occurred from the Florida Atlantic Coast to the Texas Gulf Coast, has been analyzed in detail (Flanagan et al., 2016). The present study included an additional four freshwater sites from Texas, Louisiana, Alabama, and Florida (Fig. 1A), which were analyzed and compared to the marine sites. At each sampling site (marine and freshwater) we measured the salinity of the water with a refractometer to verify our assignment of sites as freshwater or saltwater. The freshwater sites were in Texas (TXFW), Louisiana (LAFW), Alabama (ALFW), and Florida (FLFW). Approximately 50 fish were collected from each site by pulling a push net through submerged vegetation. Once fish were collected, each fish was photographed while alive before being sacrificed and preserved on dry ice for DNA analysis. Samples remained frozen on dry ice until transfer to -80°C freezers.

Phenotype analyses

The photographs of pipefish were analyzed with ImageJ (Rasband, 1997), which was used to measure phenotypic traits, including tail length, snout-vent length (SVL), body depth, snout length, head length not including snout length, and snout depth. Two female traits previously shown to experience sexual selection, band area and band number (Flanagan et al., 2014), were also measured using the program tpsDig2 (Rohlf, 2005). A principal components analysis was conducted using the R (R Core Team, 2017) package vegan (Oksanen et al., 2015) to identify the major traits contributing to variation among populations.

Sequencing library preparation

To prepare sequencing libraries we used a modified double-digest restriction site associated DNA sequencing protocol, (ddRADseq, Peterson, Weber, Kay, Fisher, & Hoekstra, 2012), with slight modifications as described in Flanagan et al. (2016). The preparation of sequencing libraries containing the saltwater sites is described in Flanagan et al. (2016), and the freshwater sites were prepared using the same methods in parallel with the marine populations. The freshwater populations comprised two full libraries, which were sent to the University of Oregon Genomics Core Facility for single-end sequencing on an Illumina Hi-Seq 2000 machine.

Generating and filtering RAD loci

The processing and mapping of reads and genotype calling methods used for this study were the same as those in Flanagan et al. (2016), only with the freshwater individuals included for SNP calling. To summarize, we used process_radtags in Stacks v. 1.29 (Catchen, Hohenlohe, Bassham, Amores, & Cresko, 2013; Catchen, Amores, Hohenlohe, Cresko, & Postlethwait, 2011) to process the reads before mapping them to a draft version of the *S. scovelli* genome (Small et al., 2016) using bowtie2.0 with the 'sensitive' parameters (Langmead & Salzberg, 2012). Following mapping, we used ref_map.pl in Stacks v. 1.29 (Catchen et al., 2013; Catchen et al., 2011) to generate a catalog of RAD loci using all 16 populations (12 marine and 4 freshwater), requiring a minimum coverage of 3x and allowing two mismatches in generating the catalog. From these 100-bp RAD loci, the multinomial likelihood model in Stacks identified the two most frequently observed nucleotides at each SNP position (Catchen et al., 2013).

The populations module in Stacks v. 1.40 (Catchen et al., 2013) was used to calculate population genetics statistics and also to filter the data. We included biallelic SNPs that were found in all of the 16 populations, in 75% of the individuals, and that had a minor allele frequency of at least 5%. We used the R package radiator (Gosselin, 2019) to filter out individuals and SNPs with low coverage, remove SNPs that did not pass Hardy Weinberg Equilibrium tests at a 0.05 threshold within each population, and to select one SNP per RAD locus to reduce the effects of linkage disequilibrium due to physical linkage. This dataset will be referred to as the 'full' set of SNPs.

We also ran the populations module of Stacks v. 1.40 including only the freshwater populations and their nearest neighboring saltwater populations (TXCC, TXFW, LAFW, ALFW,

ALST, FLCC, FLFW) for pairwise comparisons. For this run, we required loci to be present in all populations and in at least 75% of the individuals at a minimum frequency of at least 5%. Again, we kept one SNP per locus (this is the 'subsetted' dataset). We subsequently ran populations another time to extract the subsetted loci from all 16 populations (i.e., using a whitelist).

Analysis of population structure

To identify overall similarity between populations, we analyzed the 'full' SNP set (containing data from all 16 populations) in a number of ways. We used fixation indices as a metric of population structure, using the mean pairwise F_{ST} statistics calculated by Stacks. We also evaluated the covariance between populations as measured by Treemix (Pickrell & Pritchard, 2012). Additionally, we plotted the distributions of minor allele frequencies in each population using the gwscaR package (https://github.com/spflanagan/gwscaR)(Flanagan & Jones, 2017).

We used ADMIXTURE (Alexander, Novembre, & Lange, 2009) to estimate the ancestry of individuals, testing cluster values of $K=1$ through $K=16$. The optimal number of clusters, K, was determined by choosing the K associated with the lowest cross-validation error. The output was visualized using custom R scripts.

We also used a principal components analysis (PCA) to analyze population structure because it has been demonstrated to be effective in cases of isolation by distance (Engelhardt & Stephens, 2010) and the marine populations used in this study were previously shown to have a strong isolation-by-distance pattern (Flanagan et al., 2016). We used PCAdapt (Duforet-Frebourg, Bazin, & Blum, 2014), which conducts a PCA and uses the number of informative eigenvalues to infer population structure.

Analysis of demographic structure

To infer population splits and migration events among populations we used Treemix v. 1.13 (Pickrell & Pritchard, 2012) with our full dataset (7433 SNPs). This program builds maximum likelihood trees from covariances among populations using blocks of SNPs, and in all of our analyses we used block sizes of 100 SNPs. We first ran 100 bootstraps without a root and with 0 migration events, and built a consensus tree using PHYLIP v. 3.697 (Felsenstein, 2005). After inspecting the consensus unrooted tree (S1), we set FLAB as the root and ran 100 bootstraps with 0 migration events and generated another consensus tree using PHYLIP v. 3.697 (Felsenstein, 2005). Using this rooted

consensus tree, we then ran 100 bootstraps with 0-5 migration edges and estimated the maximum likelihood trees (i.e, without the -bootstrap flag) and calculated standard errors. From these bootstraps with 0-5 migration edges, we chose the optimal number of migration edges using the Evanno method (Evanno, Regnaut, & Goudet, 2005) as implemented in the R package optM (Fitak, 2019). For the chosen number of migration edges, we checked the most commonly occurring migration edges in the bootstraps and confirmed that they matched the migration edges in the maximum likelihood tree (see Results and S1 for details). In addition, we tested for treeness using the f3 and f4 tests with blocks of 100 SNPs and FLAB as the root. We evaluated the corresponding f3 and f4 outputs for the resulting migration edges to determine whether those edges are indicative of gene flow or admixture (see S1).

Analysis of demographic history

To investigate the demographic history of our populations, we used $\delta_A\delta_I$ version 1.7.0 (Gutenkunst et al., 2009). We estimated folded joint site frequency spectra for each pair of nearest freshwater-saltwater population pairs (i.e., FLFW vs. FLCC, ALFW vs. ALST, LAFW vs. ALST, and TXCC vs. TXFW), as we lacked a clear outgroup. For each population pair, we re-filtered the output from the ref_map.pl Stacks module to retain independent SNPs (one SNP per RAD locus) found in 90% of all individuals in each population, without an allele frequency cutoff. Furthermore, when running $\delta_A\delta_I$ we projected our data down (i.e., decreased our sample size of individuals) to 30 sites (or 15 individuals) in each population to account for missing data (the actual number of individuals were: FLFW=35, FLCC = 30, ALFW=36, ALST=35, LAFW=36, TXCC=23, and TXFW=30).

For each group of populations we tested the 26 two-dimensional demographic models modified for folded spectra from Rougeux et al. (2017) by Rougemont et al. (2020), and we used the optimization methods from Portik et al. (2017) to optimize the fit of each model. The 26 models (Fig. S2.1) were chosen because they are models of four alternative types of divergence (strict isolation, secondary contact, isolation with migration, and ancient migration) plus extensions of these models that included (a) temporal variation in effective population sizes, (b) two types of loci to capture the effects of selection at linked sites, (c) heterogenous migration across the genome, and (d) combinations of those three. See Rougeux et al. (2017) and Rougemont et al. (2020) for details on the implementation of the models.

For each population pair, we first ran the simplest versions of the models (SI, IM, AM, and SC) 21 times, with each replicate including a total of 100 runs across 4 rounds (as recommended by Portik et al. (2017)). To compare the fit of these four models to each population pair, we first identified the replicate with the median log-likelihood (i.e., the best run for each model was the run with the median log-likelihood). We opted to use the median because we noticed that some replicates of our models resulted in extreme parameter estimates not representative of the other replicates (Fig. S2.3). Because our dataset included only a single SNP per RAD locus, we treated our loci as unlinked and therefore used log-likelihood values to compare models, relying on the Akaike information criterion to assess model fits. To identify the simple model with the best fit while correcting for the number of parameters, we calculated ΔAIC values for the chosen replicate for each model i as AIC_i - AIC_{min} (where i={1..number of models}). The simple models with ΔAIC ≤ 10 were identified as the baseline demographic scenarios best fitting our dataset, and we then ran at least 17 replicates of each of the extended models for that scenario (see S2 for details).

We then compared the fit of the extended models using AIC scores, Akaike weights, and model scores for the replicate with the median log-likelihood following the methods of Rougeux et al. (2017). From the ΔAIC values, we computed Akaike weights, w_{AIC}, using the formula:

$$w_{AIC} = \frac{e^{\frac{-\Delta AIC_i}{2}}}{\Sigma_{i=1}^{R} e^{\frac{-\Delta AIC_i}{2}}}.$$

We also calculated scaled model scores within each population pair to facilitate model comparisons, using the equation: $model\ score = \frac{\Delta_{max} - \Delta AIC_i}{\Delta_{max}}$, where $\Delta_{max} = AIC_{max}$ - AIC_{min}. The best models for each population pair were those with the highest model scores, the highest w_{AIC} values, and the lowest ΔAIC. Parameters of the best models were not transformed into biologically meaningful estimates because our goal was to perform model selection among demographic scenarios, and parameter values should be estimated through bootstrapping to obtain confidence intervals (Gutenkunst et al., 2009; Portik et al., 2017).

Identifying outliers associated with local adaptation

We identified SNPs with outlier AMOVA-corrected F_{ST} values in pairwise comparisons of each freshwater population and its nearest saltwater neighbor (TXFW-TXCC, LAFW-ALST, ALFW-

ALST, FLFW-FLCC; see Fig. 1) using the subsetted dataset. Outliers were identified as those SNPs with a Fisher's P-value less than or equal to 0.05, as calculated by populations (Catchen et al., 2013). We then identified SNPs that were shared among all four pairwise comparisons. As a control, we performed the same pairwise comparisons between the saltwater populations and their nearest neighbors (TXCC-TXCB, ALST-FLSG, FLCC-FLPB) to identify any overlapping SNPs in those comparisons. Due to the high degree of differentiation between the Florida freshwater and saltwater populations, we used outliers shared among the TXFW-TXCC, LAFW-ALST, and ALFW-ALST pairwise comparisons in downstream analyses (see Results).

We also calculated F_{ST} values between the saltwater-freshwater pairs and permuted the population labels. We wrote custom R functions (see fwsw_supplement3.Rmd) to permute the population labels 1000 times and identified loci that had 'true' F_{ST} values outside of the range of permuted F_{ST} values. To estimate pairwise F_{ST} we used gwscaR (https://github.com/spflanagan/gwscaR; Flanagan & Jones, 2017). Loci with values outside their permuted ranges are more likely to be truly reflective of differences in allele frequencies between the two populations.

Furthermore, we used PCAdapt to identify outliers. Using the subsetted dataset, we identified the number of clusters using the screeplot (Supplementary File 2). We identified $K = 4$ as the number of clusters to the left of the straight line of points, and therefore used that as our number of clusters. Using this value, we used the qvalue package (Storey, Bass, Dabney, & Robinson, 2019) to calculate q-values from the PCAdapt p-values, which allowed us to identify outliers with a false discovery rate of $\alpha = 0.05$.

Because the signatures of selection of interest are a result of adaptation to a new ecological niche (freshwater habitats), we tested for isolation by ecology using the gene-environment association analysis implemented in BayEnv2 (Coop, Witonsky, Di Rienzo, & Pritchard, 2010; Günther & Coop, 2013). We converted the subsetted dataset (with only the freshwater-saltwater population pairs) into the appropriate input format using PLINK 1.07 (Purcell et al., 2007) and then estimated ten separate matrices. We visually inspected the matrices and, upon determining that the estimated matrices were qualitatively similar (Fig S3.14 and S3.16), we chose one representative matrix to use in the downstream analyses. Using this representative matrix to account for population structure, we

assessed the correlation between each SNP in the dataset to three different environmental variables, all of which were measured at the sample site on the day we collected the fish: the salinity, the surface water temperature, and an estimation of submerged vegetation coverage at the site (measured on a scale from 1 to 5, with 5 being complete coverage). These values were standardized by subtracting the mean and dividing by the standard deviation. Although BayEnv2 provides different metrics for interpreting the correlations, we focused on the Bayes Factors because they have higher power than the Spearman rank coefficients (Lotterhos & Whitlock, 2015). We performed the Bayenv2 analysis twice, once with all seven populations in the subsetted dataset, and once without the Florida populations.

Results

No major morphological differences were observed between freshwater and saltwater populations (Fig. S1.1). The majority of the variation in both male and female body traits was explained by the first principal component (95.27% of variation in males and 90.95% of variation in females), for which tail length had the highest loading for both sexes (males: 0.8044, females: 0.7643; Table S1.1). The second principal component explained 4.11% of the variation in male body traits and 7.73% of the variation in female body traits and mainly reflects variation in SVL (males: -0.7976, females: 0.7676; Table S1.1). These results indicate that individuals in some populations were larger than others, which is consistent with the results in Flanagan *et al.* (2016). The female band traits (band number and mean band area) display most variation in band number, with band number loading on PC1 (Band Number PC1 loading = -0.9997) and PC1 explaining 98.38% of the variation.

A total of 194,294 RAD loci were identified by Stacks. The average coverage per locus was 6.6x and individuals had an average coverage of 9.5x. The full dataset, which contained loci passing coverage and Hardy-Weinberg thresholds and found in all 16 populations and 75% of individuals, contained 7433 RAD loci, with one SNP per locus, and 605 individuals. The subsetted dataset, with only individuals from the freshwater populations (TXFW, ALFW, LAFW, FLFW) and their nearest saltwater neighbors (TXCC, ALST, FLCC) contained 12103 SNPs at 12103 RAD loci. These two datasets had comparable observed heterozygosity, minor allele frequencies, and percent polymorphic loci for the seven populations in the subsetted dataset (Table 1).

Population structure

Pairwise F_{ST} values between the 16 populations range from 0.007 to 0.254 (mean 0.047). The most extreme pairwise F_{ST} is between the two most distant freshwater populations, TXFW and FLFW, with an average pairwise F_{ST} value of 0.254 (calculated from the full dataset by Stacks; Table 2, Figure S1.2). Both of these populations are also divergent from nearby saltwater populations (TXFW vs TXCC F_{ST} = 0.0386; FLFW vs FLCC F_{ST} = 0.1336; Table 2). Examining the allele frequency spectra (Figure S1.3), these two populations exhibit decreased genetic diversity, with more alleles fixed, particularly in FLFW (Table 1). These skewed allele frequency spectra are reflected in the high F_{ST} values (Figure S1.2). The other two freshwater populations, ALFW and LAFW, are more homogeneous with nearby saltwater populations, in particular their shared nearest neighbor, ALST. The most similar populations are groups of saltwater populations nearest to each other, grouped generally by coast (Florida Atlantic Coast, Florida Gulf Coast, Texas Gulf Coast), consistent with the findings in Flanagan et al. (2016).

The analysis of individual ancestries with ADMIXTURE revealed both *K*=5 and *K*=7 to have similarly low cross-validation error rates (0.10962 and 0.10822, respectively; Figure S1.4; see Figures S1.5-S1.10 for plots of *K*=2 through *K*=7). The analyses with these two numbers of clusters result in similar ancestry assignments, but when *K*=7 the TXFW and FLAB populations each have their own cluster, unlike in *K*=5 (Fig. 1C). In both cases, the Florida freshwater population (FLFW) is in a cluster of its own. The Alabama saltwater population (ALST) is in the same cluster as the Alabama and Louisiana freshwater populations (ALFW and LAFW), but appears to have low levels of admixture with the Florida east coast cluster (Fig. 1C).

The optimal number of clusters identified by PCAdapt with the full dataset was 7 (Fig. S1.11), in line with the ADMIXTURE analysis. The first four PC axes describe 80.31% of the variation among genotypes, with the first axis (33.26% of variation) separating the Florida east coast from the other populations. The second axis (20.25% of variation) primarily partitions the Florida freshwater population from the Florida east coast marine populations. The third axis of variation (16.71%) partitions the Texas and Florida Gulf coast populations, and the fourth axis (10.09%) divides the marine and freshwater populations within their geographic clusters (Fig. 1D, Fig. S1.12, Table S1.2).
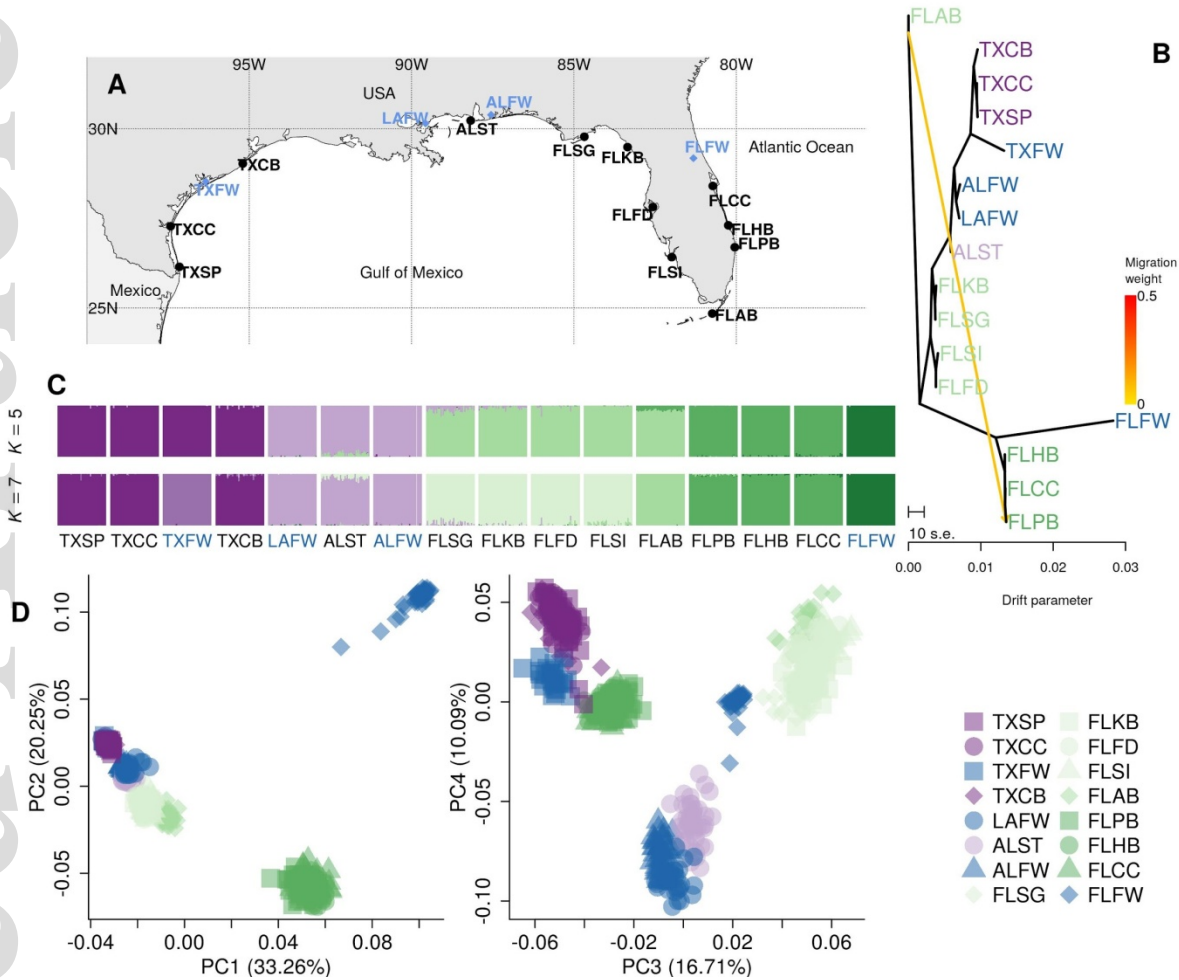
Figure 1. The collection locations of the marine populations (black circles) and the freshwater populations (blue diamonds) on a map of the southeastern USA (**A**). One migration event is supported in the treemix analysis, from the branch between FLAB (the root) and the other populations leading to FLPB. (**B**). The ADMIXTURE results for two runs with similarly low error rates, *K*=5 and *K*=7, reflect the pattern of isolation by distance described in Flanagan *et al.* (2016) and reflects the branching patterns in the treemix analysis (**C**). The PCAdapt analysis with *K*=7 clusters reveals that the first axis of variation explains differences between the east coast of Florida and the rest of the populations and the second axis of variation separates the Florida freshwater population from the others, and the next two axes split apart populations by geographic location and freshwater or saltwater status (**D**).

Demographic structure

        After inspecting the unrooted consensus tree from treemix, we chose FLAB as the root to create a consensus tree (Fig. S1.13) and tested 0 to 5 migration edges on the population tree. One migration edge resulted in the lowest amount of error (Fig. S1.14, S1.15). This migration edge represents gene flow between FLAB and FLPB (Fig. 1B, Fig. S1.16, Table S1.3, Table S1.4), reflecting the low levels of admixture observed in the ADMIXTURE analysis with 5 clusters (Fig. 1C). The f3 and f4 treeness analyses support this admixture to some extent. Although none of the three-population trees including FLAB and FLPB are substantially negative (i.e., standard errors not overlapping zero), the trees with FLPB as an outgroup to FLAB and another Atlantic-coast Florida population (i.e., those in the form [FLPB [FLAB,FLCC or FLHB or FLLG]]) have estimates that are negative (Fig. S1.17). All of the four-population trees including FLPB, FLAB, and two other east coast Florida populations have substantially positive f4 statistics (Fig. S1.18, Table S1.5), which suggests that those four-population trees have evidence of admixture among the populations.

Demographic history

        The results from $\delta_A\delta_I$ reveal different demographic histories for freshwater populations found in bays versus those found in isolated lakes, although all include some extent of contemporary migration with nearby marine populations (Fig. 2, S2). The best demographic models for the Florida and Texas population pairs were clearly models based on isolation with migration, this IM model being the only one with a ΔAIC<10 (a typical threshold , e.g. Portik et al., 2017; Rougemont et al., 2017, 2020) for the simple models (Fig. S2.2, S2.13, Tables S2.3, S2.9). The Louisiana comparison also only had one simple model as a clearly best model, and that was a model with secondary contact (Fig. S2.10, Table S2.7). However, for the Alabama populations both the isolation with migration and secondary contact models fit the data well (ΔAIC < 10, Table S2.5), so the extensions of both of those models were run.

        All of the population pairs had one clearly best-fitting extended model, with the exception of the Florida populations. The FLFW vs. FLCC models had both the isolation with migration and IM2m (isolation with migration with heterogeneous migration rates genome-wide) models with ΔAIC<10 (Table S2.4), but the isolation with migration model had a slightly better fit despite having fewer parameters so we present that model in Fig. 2. The best-fitting model for both ALFW-ALST

and LAFW-ALST was SC2mG (secondary contact with heterogeneous migration rates genome-wide and changes in population size; Fig 2, S2.7, S2.8, S2.11, Tables S2.6, S2.8), and for TXFW vs. TXCC the IM2m model provided the best fit (Fig. 2, S2.15, Table S2.10).
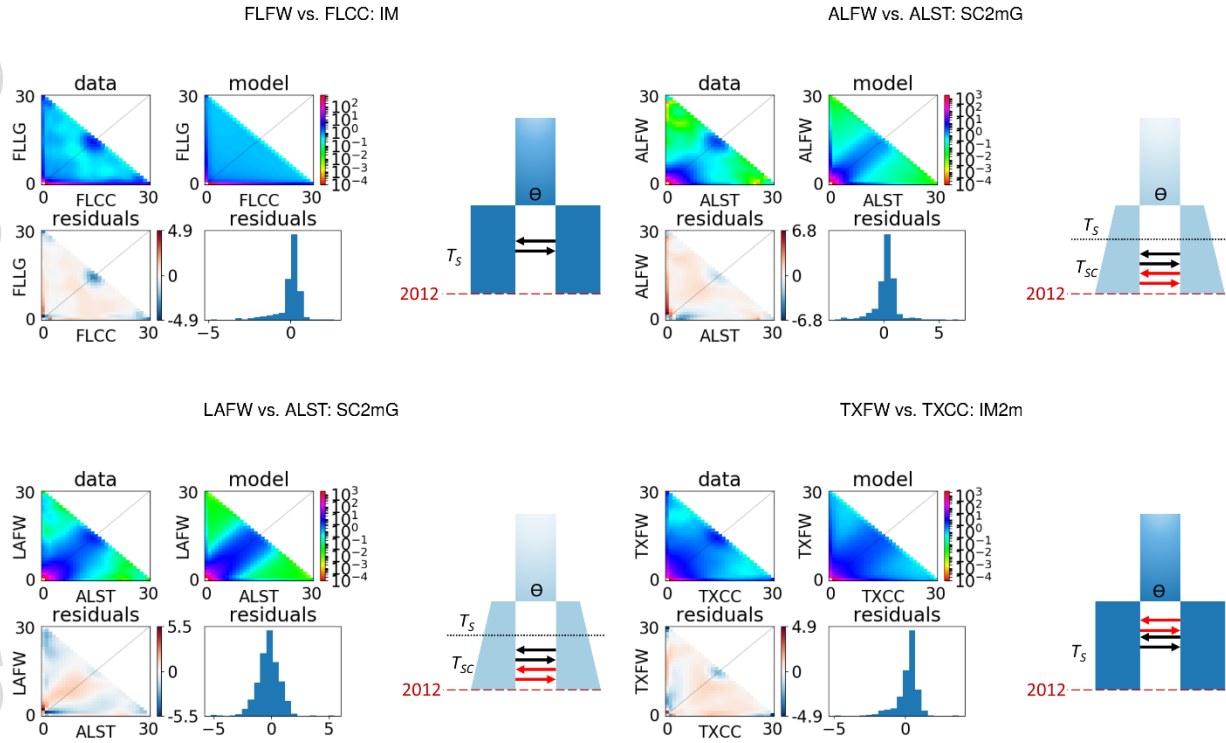

Figure 2. The best-fitting $\delta_A\delta_I$ models for each freshwater population and its nearest saltwater neighbor. Shown for each pair are the two-dimensional joint frequency spectrum for the data versus the model along with the residuals for each model. To the right of those four plots are schematics for the best fitting model. Counterclockwise from top left, the comparisons are: FLFW vs. FLCC (best model: isolation with migration); ALFW vs. ALST (best model: secondary contact with heterogeneous migration rates genome-wide and changes in population size); LAFW vs. ALST (best model: secondary contact with heterogeneous migration rates genome-wide and changes in population size); TXFW vs. TXCC (best model: isolation with migration with heterogeneous migration rates genome-wide). For more information see Supplement 2.
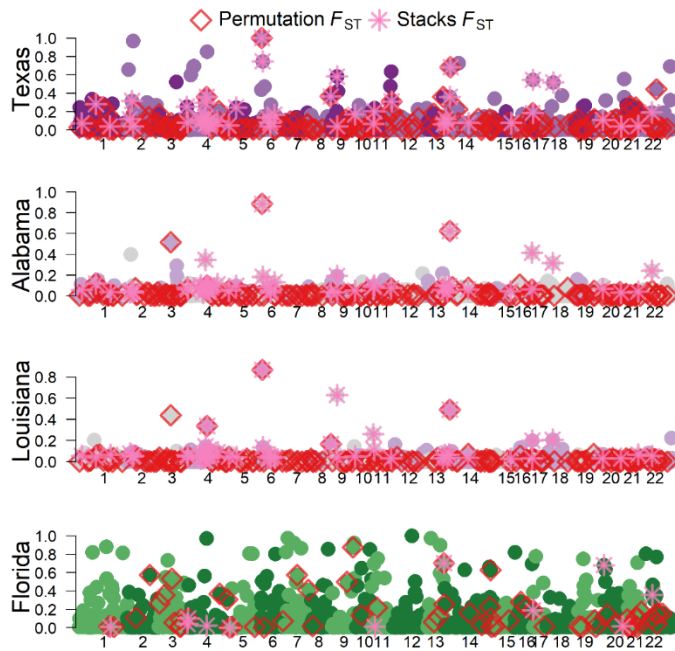
Shared outliers associated with salinity

We looked for shared patterns of adaptation to freshwater environments using the subsetted dataset (only the freshwater populations and their nearest marine neighbors). Using the Stacks AMOVA-corrected F_{ST} values, we found 7 SNPs on five chromosomes that had a p-value < 0.05 in
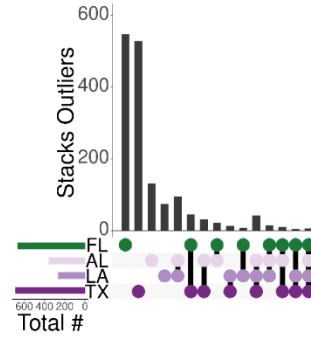
all four pairwise comparisons. However, the Florida pairwise comparison included many SNPs with large F_{ST} values, likely due to genetic drift, meaning that its distribution was over-saturated for identifying outliers. Therefore, we focused on the 50 SNPs on 17 chromosomes that had a *p*-value < 0.05 in the TXFW-TXCC, LAFW-ALST, and ALFW-ALST comparisons (Fig. 3, S3). A total of 17 SNPs (on 10 chromosomes and 3 unanchored scaffolds) had F_{ST} values outside the permuted distributions in all four pairwise comparisons, but none of these overlapped with the shared Stacks F_{ST} outliers (S3). For consistency with the Stacks analysis, we focused our attention only on the shared outliers from the Texas, Louisiana, and Alabama comparisons, and found 215 shared outliers on all 22 linkage groups (Fig. 3, S3). Of these outliers, 13 overlapped with the shared Stacks outliers (Fig. 4, S3).

PCAdapt and Bayenv also identify outliers after correcting for population structure. Of the 12103 SNPs, 140 were significant in the PCAdapt analysis located on all 22 chromosomes (we focus here on the analysis without the Florida populations, but present the analysis with all 7 populations in S3). The X^TX analysis contained 108 outliers on 20 chromosomes (Table S3.6). Three of these were also identified by the X^TX analysis in Bayenv2, one of which was also an outlier in the salinity association analysis (Fig. 4), and four with the permutation analysis. None of the PCAdapt outliers were also shared outliers in the Stacks analysis (S3).
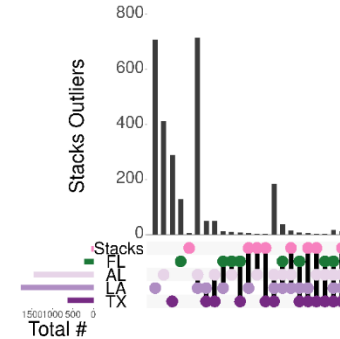
Figure 3. In **(A)** are the pairwise AMOVA-corrected F_{ST} values for each freshwater-marine comparison calculated by Stacks. The top panel shows the Texas comparison, the second the Alabama comparison, the third the Louisiana comparison, and the bottom panel shows the Florida comparison. In each panel the alternating colors represent different chromosomes, which are numbered along the x-axis. The 50 SNPs that were outliers in all Stacks F_{ST} comparisons (except Florida) are marked with pink asterisks and the SNPs that were significant in all three permutation analyses are marked with red diamonds. Note that some outliers are not pictured as they are on unanchored scaffolds. The upset plot in **(B)** shows the overlap among the four pairwise Stacks F_{ST} comparisons, highlighting that 7 SNPs are outliers in all four comparisons, but that most overlap occurs between Louisiana, Alabama, and Texas. The upset plot in **(C)** shows similar patterns for the permutations, and also identifies the overlap between the permutation analyses and the outliers shared in the pairwise Louisiana, Alabama, and Texas Stacks analysis ('Stacks' does not include Florida).

We also investigated correlations between genetic variation and salinity using Bayenv and found 108 SNPs with significant associations with salinity. These SNPs were distributed across the genome, representing all 22 linkage groups and 20 unanchored scaffolds. The salinity-associated SNPs overlapped with 16 of the X^TX outliers, and three shared Stacks outliers (but none shared permutation outliers; Fig. 4).

The outliers from all analyses were distributed genome-wide without clear clustering in any one genomic region (Figs 3, 4). Nonetheless, several outliers on LG6 were consistently identified by the F_{ST} outlier analyses, the X^TX analysis, and the salinity association analysis. These outliers spanned 6.13 Mb. Eight outlier SNPs on LG6 were in coding regions, 1 was in a regulatory region (3' or 5' untranscribed regions), and 4 were in un-annotated regions of the linkage group. One SNP was an outlier in all 3 Stacks F_{ST} analyses, the permutations, X^TX, and salinity-associated analyses and this SNP was located in a coding region for the *leucine-rich repeat and coiled-coil domain-containing protein 1* (*LRRCC1*). Outliers from all analyses were not more likely to be located in coding regions, regulatory regions, or non-coding regions compared to the overall distribution of SNPs (Fisher's exact test, $p = 0.993$; S3). Similarly, outliers were not enriched in genes putatively associated with freshwater adaptation (Fisher's exact test, odds ratio = 1.403, $p = 0.123$; see Table S3.10 for the list of putative genes).
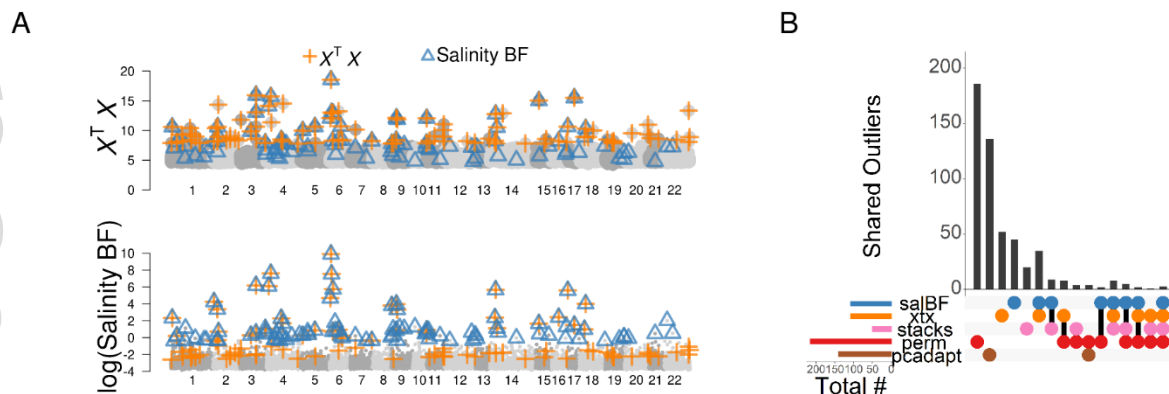
Figure 4. In **(A)**, the genome-wide distribution of Bayenv X^TX values (top panel of A) and the logarithm of the Bayes Factors associated with salinity in Bayenv (bottom panel of A) are shown. Alternating light and grey points represent the chromosomes, which are numbered along the x-axis. Bayenv X^TX outliers are marked with an orange +; and salinity-correlated outliers are marked with a blue triangle. In **(B)**, the overlap in outliers among analyses is shown in an upset plot.

Discussion

Our population genetic, demographic structure, and demographic history analyses reveal that geography plays a major role in determining gene flow in both freshwater and saltwater populations of *S. scovelli*. The majority of variation among populations is due to geographical proximity for both freshwater and saltwater population (Fig. 1), and the best-fitting demographic models show that some populations appear to have colonized freshwater habitats despite recent gene flow with nearby saltwater populations, while others seem to involve more complex histories of secondary contact (Fig. 2, S2). Even though the demographic models suggest that recent or ancestral migration has occurred between populations, we found limited evidence of genetic parallelism among freshwater populations (Fig. 3). Additionally, despite identifying heterogeneous migration rates across loci in the demographic models, we did not identify any large regions of the genome with a concentration of loci associated with salinity in any freshwater populations (Fig. 4), although the Florida freshwater population was sufficiently differentiated from its nearest saltwater neighbor that identifying shared signals of adaptation was challenging (Fig. 3). These results together suggest that these euryhaline fish are able to repeatedly colonize habitats that vastly differ in salinity.

The overall patterns of population differentiation reveal the importance of geography in structuring Gulf pipefish populations. The primary factors driving population clustering were geographic, with the populations from the Gulf of Mexico clearly separating from the Atlantic populations (Fig. 1, Table 2). The four freshwater populations of *S. scovelli* also showed geographic clustering, with the Alabama and Louisiana freshwater sites grouped together with evidence of shared genetic variation (Fig. 1). These results are consistent with both their positions in bays and with previous work focused on the Alabama freshwater and saltwater populations (Partridge et al., 2012). The single migration edge supported by the Treemix analysis indicates that the population in the Florida Keys -- on the boundary between the Atlantic populations and the Gulf of Mexico populations -- might serve as a link between these two groups. This important role of geography in our study is consistent with our previous interpretation of isolation-by-distance driving population differentiation in the saltwater populations (Flanagan et al., 2016) and with the relatively low rates of gene flow from the Gulf of Mexico to the Atlantic found by Bertola et al. (2020).

Intriguingly, the demographic models that best fit the populations in isolated lakes (TXFW and FLFW) supported a model of ongoing migration whereas the populations in bays (ALFW and LAFW) were best fit by models of secondary contact (Fig. 2). Furthermore, only ALFW and LAFW showed evidence of genetic bottlenecks, as their best-fitting demographic models included a growth parameter (Fig. 2, S2). These results are surprising given that the Texas freshwater site is in the Lake Texana reservoir, which is cut off from the ocean by a dam (Martin et al., 2013) and the Florida freshwater site is isolated from the ocean by approximately 100 river miles (McLane, 1955) and is north of the point where the Gulf stream veers away from the east coast of Florida, which creates a biogeographic barrier that has been implicated as a driver of population structure in other syngnathids (Bertola et al., 2020; Boehm, Waldman, Robinson, & Hickerson, 2015; Mobley, Small, Jue, & Jones, 2010). How individual fish might move into these isolated freshwater systems is unknown, but possibilities include human-facilitated transport in bait buckets (Martin et al., 2013), rafting on Sargassum (Bertola et al., 2020), and via flooding during hurricanes and tropical storms (Piazza & La Peyre, 2009). One possible explanation for the results of the demographic models is that the isolation of these populations is too recent (e.g., within the past 100 years) for models of extended periods of geographic isolation to fit the data.

All population pairs were well-fitted by models including heterogeneous migration rates throughout the genome (i.e., the inclusion of the 2m parameter, with estimates of proportions of the genome evolving neutrally ranging from 0.4870 to 0.9376 in best-fitting models; S2). Barrier loci in demographic models including a long period of isolation without migration, such as secondary contact models, are often interpreted to arise due to the accumulation of genetic incompatibilities between populations (e.g., Le Moan et al., 2016; Portik et al., 2017; Rougemont & Bernatchez, 2018; Rougeux et al., 2017; Tine et al., 2014). Thus, we could interpret our demographic model results to suggest that the Alabama and Louisiana freshwater populations might be diverging from their marine neighbours due in part to intrinsic barriers. On the other hand, the Texas population -- and to a lesser extent the Florida population -- is best fit by a model with ongoing migration, in which case heterogeneous migration rates might be better inferred as arising due to divergent selection pressures or other extrinsic barriers to migration (Ravinet et al., 2017). The Florida and Texas freshwater sites also show higher levels of divergence from nearby saltwater sites, potentially indicating an important role for

divergent ecological selection in generating barrier loci in these populations. Thus, our demographic models suggest that different mechanisms could be leading to divergence in each freshwater population.

Despite the potential for multiple mechanisms creating barrier loci in our populations, patterns of genetic parallelism were found genome-wide in both coding and non-coding regions (Fig. 3, 4; S3). One locus with particularly high values in all analyses -- including the Bayenv analyses with the Florida populations (S3) -- is within the gene *leucine-rich repeat and coiled-coil domain-containing protein 1* (*LRRCC1*), which is associated with centrosomes (Muto & Okano, 2010; Ruzicka et al., 2019) and has not previously been identified in the context of freshwater adaptation. This locus itself may not be a target of selection, as it might be subject to genetic hitchhiking or reduced recombination rates, but its consistent presence as an outlier suggests that this region of LG6 might play a role in freshwater adaptation in pipefish. The genetic parallelism between the Alabama and Louisiana freshwater populations was particularly distinct, and given both the important role of heterogeneous migration and a secondary contact model in the demographic results, these two populations could be consistent with the transporter hypothesis (Schluter & Conte, 2009), with freshwater-beneficial mutations spread among these two freshwater populations via the saltwater populations.

Despite our demographic models suggesting reduced migration at some loci and some shared outliers, patterns of genetic parallelism were not localized in any one particular genomic region (Fig. 3,4, S3). Nonetheless, several shared outliers were found in one 6.13Mb region on LG6, and this region could be indicative of a genomic island of divergence. However, our RAD-seq data contained 248 additional SNPs within this region that did not show evidence of population differentiation in freshwater populations (S3). We therefore did not find overwhelming evidence for islands of divergence, as have been found in other studies (Christmas et al., 2018; Hohenlohe, Bassham, Currey, & Cresko, 2012; Le Moan, Bekkevold, & Hemmer-Hansen, 2020; Marques et al., 2016; Renaut et al., 2012; Riquet et al., 2019; Westram et al., 2018), most notably in the repeated colonization of freshwater habitats by threespine sticklebacks (Deagle et al., 2012; Jones et al., 2012). Genomic islands might yet exist in pipefish, either as regions of reduced recombination (Cruickshank & Hahn, 2014; Noor & Bennett, 2009) or as inversions containing multiple adaptive loci (Mérot, Oomen,

Tigano, & Wellenreuther, 2020; Wellenreuther & Bernatchez, 2018), but our dataset of 12103 SNPs may not have been dense enough to detect genomic islands. Alternatively, changes in gene expression in response to salinity impacts immune response in pipefish (Birrer, Reusch, & Roth, 2012) and could determine the ability to survive and reproduce in freshwater (e.g., Wang et al., 2020). The associated changes in regulatory regions or epigenetic patterns would not likely be captured in islands of divergence. This alternative explanation is particularly intriguing for *S. scovelli*, as the species is euryhaline (Bolland & Boettcher, 2005; Partridge et al., 2012) and thus even saltwater populations are able to regulate the osmolarity in their brood pouches (Quast & Howe, 1980) and otherwise tolerate low salinities (Partridge, Cazalas, Rozelle, Hemming, & Boettcher, 2004).

The finding that gene flow underlies each of these colonizations of freshwater habitats by the Gulf pipefish is in some ways similar to patterns of colonization of freshwater by other marine fish, such as sticklebacks (Deagle et al., 2012; Jones et al., 2012; Rennison et al., 2020), European anchovy (Le Moan et al., 2016), and lamprey (Rougemont et al., 2017). However, although genetic parallelism, likely arising through recent gene flow, is important in our results, the factor explaining most of the variation in our dataset is geography (Fig. 1). This overarching importance of geography has also been demonstrated in other systems, including threespine sticklebacks (Rennison et al., 2020), *Anolis* lizards (Gray et al., 2019), and corkwing wrasse (Mattingsdal et al., 2020). This importance of neutral processes in population differentiation in *S. scovelli* is reflected in previous analyses of saltwater populations (Bertola et al., 2020; Flanagan et al., 2016; Partridge et al., 2012).

Our results suggest that geographic isolation and evolutionary histories might be more important in shaping genetic divergence than ecological selection, but that different mechanisms might underpin divergence in each population. Nevertheless, our demographic models provided evidence for barrier loci and genetic parallelism playing key roles in population divergence. Together, our results highlight that the colonization of new habitats involves a suite of complex evolutionary mechanisms, including genetic drift, heterogeneous migration rates, and ongoing gene flow.

Data Accessibility

Raw sequencing data are available from the NCBI Sequence Read Archive (Accession no. SRP077648). Phenotypic data, collecting site data, and genotype files are archived on Dryad (https://doi.org/10.5061/dryad.12jm63xvh, URL for review: https://datadryad.org/stash/share/PIBkFdjwiV1eNkhP8_pRFcjkP0vwVbvxPjmD5PyDoEA). All code and scripts used in the analyses are archived on Zenodo (DOI: 10.5281/zenodo.4528951) can be downloaded from GitHub (https://github.com/spflanagan/popgen/releases/tag/v2.2) or can be obtained by contacting the authors.

Conflict of Interest

The authors have no conflicts of interest to declare.

References

Alexander, D. H., Novembre, J., & Lange, K. (2009). Fast model-based estimation of ancestry in unrelated individuals. *Genome Research*, *19*(9), 1655–1664. doi: 10.1101/gr.094052.109

Barton, N. H. (1979). The dynamics of hybrid zones. *Heredity*, *43*(3), 341–359. doi: 10.1038/hdy.1979.87

Bertola, L. D., Boehm, J. T., Putman, N. F., Xue, A. T., Robinson, J. D., Harris, S., … Hickerson, M. J. (2020). Asymmetrical gene flow in five co-distributed syngnathids explained by ocean

currents and rafting propensity. *Proceedings of the Royal Society B: Biological Sciences*, *287*(1926), 20200657. doi: 10.1098/rspb.2020.0657

Bierne, N., Welch, J., Loire, E., Bonhomme, F., & David, P. (2011). The coupling hypothesis: Why genome scans may fail to map local adaptation genes. *Molecular Ecology*, *20*(10), 2044–2072. doi: 10.1111/j.1365-294X.2011.05080.x

Birrer, S. C., Reusch, T. B. H., & Roth, O. (2012). Salinity change impairs pipefish immune defence. *Fish & Shellfish Immunology*, *33*(6), 1238–1248. doi: http://dx.doi.org/10.1016/j.fsi.2012.08.028

Boehm, J. T., Waldman, J., Robinson, J. D., & Hickerson, M. J. (2015). Population genomics reveals seahorses (*Hippocampus erectus*) of the western mid-Atlantic coast to be residents rather than vagrants. *PLoS One*, *10*(1), e0116219. doi: 10.1371/journal.pone.0116219

Bolland, J., & Boettcher, A. (2005). Population structure and reproductive characteristics of the Gulf pipefish, *Syngnathus scovelli*, in Mobile Bay, Alabama. *Estuaries*, *28*(6), 957–965. doi: 10.1007/bf02696023

Butlin, R. K., Saura, M., Charrier, G., Jackson, B., André, C., Caballero, A., … Rolán-Alvarez, E. (2014). Parallel evolution of local adaptation and reproductive isolation in the face of gene flow. *Evolution*, *68*(4), 935–949. doi: 10.1111/evo.12329

Butlin, R. K., & Smadja, C. M. (2018). Coupling, Reinforcement, and Speciation. *The American Naturalist*, *191*(2), 155–172. doi: 10.1086/695136

Carcupino, M., Baldacci, A., Mazzini, M., & Franzoi, P. (2002). Functional significance of the male brood pouch in the reproductive strategies of pipefishes and seahorses: A morphological and ultrastructural comparative study on three anatomically different pouches. *Journal of Fish Biology*, *61*(6): 1465-1480. doi: 10.1111/j.1095-8649.2002.tb02490.x

Catchen, J., Hohenlohe, P. A., Bassham, S., Amores, A., & Cresko, W. A. (2013). Stacks: An analysis tool set for population genomics. *Molecular Ecology*, *22*(11), 3124–3140. doi: 10.1111/mec.12354

Catchen, J. M., Amores, A., Hohenlohe, P., Cresko, W., & Postlethwait, J. H. (2011). Stacks: Building and genotyping loci de novo from short-read sequences. *G3: Genes, Genomes, Genetics*, *1*(3), 171–182.

Christmas, M. J., Wallberg, A., Bunikis, I., Olsson, A., Wallerman, O., & Webster, M. T. (2018). Chromosomal inversions associated with environmental adaptation in honeybees. *Molecular Ecology*, *28*(6): 1358-1374. doi: 10.1111/mec.14944

Coop, G., Witonsky, D., Di Rienzo, A., & Pritchard, J. K. (2010). Using environmental correlations to identify loci underlying local adaptation. *Genetics*, *185*(4), 1411–1423. doi: 10.1534/genetics.110.114819

Cruickshank, T. E., & Hahn, M. W. (2014). Reanalysis suggests that genomic islands of speciation are due to reduced diversity, not reduced gene flow. *Molecular Ecology*, *23*(13), 3133–3157. doi: 10.1111/mec.12796

Deagle, B. E., Jones, F. C., Chan, Y. F., Absher, D. M., Kingsley, D. M., & Reimchen, T. E. (2012). Population genomics of parallel phenotypic evolution in stickleback across stream–lake ecological transitions. *Proceedings of the Royal Society B: Biological Sciences*, *279*(1732), 1277–1286. doi: 10.1098/rspb.2011.1552

DiBattista, J. D., Saenz-Agudelo, P., Piatek, M. J., Cagua, E. F., Bowen, B. W., Choat, J. H., … Berumen, M. L. (2020). Population genomic response to geographic gradients by widespread and endemic fishes of the Arabian Peninsula. *Ecology and Evolution*, *10*(10), 4314–4330. doi: 10.1002/ece3.6199

Duforet-Frebourg, N., Bazin, E., & Blum, M. B. G. (2014). Genome scans for detecting footprints of local adaptation using a Bayesian factor model. *Molecular Biology and Evolution*, *31*, 2483–2495.

Elmer, K. R., & Meyer, A. (2011). Adaptation in the age of ecological genomics: Insights from parallelism and convergence. *Trends in Ecology & Evolution*, *26*(6), 298–306. doi: http://dx.doi.org/10.1016/j.tree.2011.02.008

Engelhardt, B. E., & Stephens, M. (2010). Analysis of population structure: A unifying framework and novel methods based on sparse factor analysis. *PLoS Genetics*, *6*(9), e1001117. doi: 10.1371/journal.pgen.1001117

Evanno, G., Regnaut, S., & Goudet, J. (2005). Detecting the number of clusters of individuals using the software structure: A simulation study. *Molecular Ecology*, *14*(8), 2611–2620. doi: 10.1111/j.1365-294X.2005.02553.x

Excoffier, L., Hofer, T., & Foll, M. (2009). Detecting loci under selection in a hierarchically structured population. *Heredity*, *103*(4), 285–298. doi: http://www.nature.com/hdy/journal/v103/n4/suppinfo/hdy200974s1.html

Felsenstein, J. (2005). *PHYLIP (Phylogeny Inference Package)*. Department of Genome Sciences, University of Washington, Seattle: Distributed by the author.

Fitak, R. R. (2019). *OptM: an R package to optimize the number of migration edges using threshold models*. Retrieved from https://cran.r-project.org/web/packages/OptM/index.html

Flanagan, S. P., Johnson, J. B., Rose, E., & Jones, A. G. (2014). Sexual selection on female ornaments in the sex-role-reversed Gulf pipefish (*Syngnathus scovelli*). *Journal of Evolutionary Biology*, *27*(11), 2457–2467. doi: 10.1111/jeb.12487

Flanagan, S. P., & Jones, A. G. (2017). Genome-wide selection components analysis in a fish with male pregnancy. *Evolution*, *71*(4), 1096–1105. doi: 10.1111/evo.13173

Flanagan, S. P., Rose, E., & Jones, A. G. (2016). Population genomics reveals multiple drivers of population differentiation in a sex-role-reversed pipefish. *Molecular Ecology*, *25*(20), 5043–5072. doi: 10.1111/mec.13794

Fogelson, S. B., Yanong, R. P. E., Kane, A., Teal, C. N., Berzins, I. K., Smith, S. A., … Camus, A. (2015). Gross, histological and ultrastructural morphology of the aglomerular kidney in the lined seahorse *Hippocampus erectus*. *Journal of Fish Biology*, *87*(3), 805–813. doi: 10.1111/jfb.12751

Gallant, J. R., Traeger, L. L., Volkening, J. D., Moffett, H., Chen, P.-H., Novina, C. D., … Sussman, M. R. (2014). Genomic basis for the convergent evolution of electric organs. *Science*, *344*(6191), 1522–1525. doi: 10.1126/science.1254432

Gompert, Z., Lucas, L. K., Fordyce, J. A., Forister, M. L., & Nice, C. C. (2010). Secondary contact between *Lycaeides idas* and *L. melissa* in the Rocky Mountains: Extensive admixture and a patchy hybrid zone. *Molecular Ecology*, *19*(15), 3171–3192. doi: 10.1111/j.1365-294X.2010.04727.x

Gosselin, T. (2019). *radiator: RADseq Data Exploration, Manipulation and Visualization using R*. 10.5281/zenodo.1475182. Retrieved from https://thierrygosselin.github.io/radiator/

Gray, L. N., Barley, A. J., Poe, S., Thomson, R. C., Oca, A. N.-M. de, & Wang, I. J. (2019). Phylogeography of a widespread lizard complex reflects patterns of both geographic and ecological isolation. *Molecular Ecology*, *28*(3), 644–657. doi: 10.1111/mec.14970

Günther, T., & Coop, G. (2013). Robust identification of local adaptation from allele frequencies. *Genetics*, *195*(1), 205–220. doi: 10.1534/genetics.113.152462

Gutenkunst, R. N., Hernandez, R. D., Williamson, S. H., & Bustamante, C. D. (2009). Inferring the joint demographic history of multiple populations from multidimensional SNP frequency data. *PLoS Genetics*, *5*(10), e1000695. doi: https://doi.org/10.1371/journal.pgen.1000695

Hill, J., Enbody, E. D., Pettersson, M. E., Sprehn, C. G., Bekkevold, D., Folkvord, A., … Andersson, L. (2019). Recurrent convergent evolution at amino acid residue 261 in fish rhodopsin. *Proceedings of the National Academy of Sciences*, *116*(37), 18473–18478. doi: 10.1073/pnas.1908332116

Hoffmann, A. A., & Sgro, C. M. (2011). Climate change and evolutionary adaptation. *Nature*, *470*(7335), 479–485.

Hohenlohe, P. A., Bassham, S., Currey, M., & Cresko, W. A. (2012). Extensive linkage disequilibrium and parallel adaptive divergence across threespine stickleback genomes. *Philosophical Transactions of the Royal Society B-Biological Sciences*, *367*(1587), 395–408. doi: 10.1098/rstb.2011.0245

Jones, A. G., Walker, D., & Avise, J. C. (2001). Genetic evidence for extreme polyandry and extraordinary sex-role reversal in a pipefish. *Proceedings of the Royal Society B-Biological Sciences*, *268*(1485), 2531–2535. doi: 10.1098/rspb.2001.1841

Jones, Adam G., & Avise, J. C. (1997). Microsatellite analysis of maternity and the mating system in the Gulf pipefish *Syngnathus scovelli*, a species with male pregnancy and sex-role reversal. *Molecular Ecology*, *6*(3), 203–213. doi: 10.1046/j.1365-294X.1997.00173.x

Jones, F. C., Grabherr, M. G., Chan, Y. F., Russell, P., Mauceli, E., Johnson, J., … Kingsley, D. M. (2012). The genomic basis of adaptive evolution in threespine sticklebacks. *Nature*, *484*(7392), 55–61. doi: http://www.nature.com/nature/journal/v484/n7392/abs/nature10944.html

Junge, C., Vøllestad, L. A., Barson, N. J., Haugen, T. O., Otero, J., Sætre, G.-P., … Primmer, C. R. (2011). Strong gene flow and lack of stable population structure in the face of rapid adaptation to local temperature in a spring-spawning salmonid, the European grayling (*Thymallus thymallus*). *Heredity*, *106*(3), 460–471. doi: 10.1038/hdy.2010.160

Kratochwil, C. F., Liang, Y., Gerwin, J., Woltering, J. M., Urban, S., Henning, F., … Meyer, A. (2018). Agouti-related peptide 2 facilitates convergent evolution of stripe patterns across cichlid fish radiations. *Science*, *362*(6413), 457–460. doi: 10.1126/science.aao6809

Langmead, B., & Salzberg, S. L. (2012). Fast gapped-read alignment with Bowtie 2. *Nature Methods*, *9*(4), 357–359. doi: 10.1038/nmeth.1923 http://www.nature.com/nmeth/journal/v9/n4/abs/nmeth.1923.html

Laugen, A. T., Laurila, A., Räsänen, K., & Merilä, J. (2003). Latitudinal countergradient variation in the common frog (*Rana temporaria*) development rates – evidence for local adaptation. *Journal of Evolutionary Biology*, *16*(5), 996–1005. doi: 10.1046/j.1420-9101.2003.00560.x

Le Moan, A., Bekkevold, D., & Hemmer-Hansen, J. (2020). Evolution at two time-frames: Ancient and common origin of two structural variants involved in local adaptation of the European plaice (*Pleuronectes platessa*). *BioRxiv*, 662577. doi: 10.1101/662577

Le Moan, A., Gagnaire, P. A., & Bonhomme, F. (2016). Parallel genetic divergence among coastal–marine ecotype pairs of European anchovy explained by differential introgression after secondary contact. *Molecular Ecology*, *25*(13), 3187–3202. doi: 10.1111/mec.13627

Lenormand, T. (2002). Gene flow and the limits to natural selection. *Trends in Ecology & Evolution*, *17*(4), 183–189. doi: https://doi.org/10.1016/S0169-5347(02)02497-7

Lotterhos, K. E., & Whitlock, M. C. (2015). The relative power of genome scans to detect local adaptation depends on sampling design and statistical method. *Molecular Ecology*, *24*(5), 1031–1046. doi: 10.1111/mec.13100

Marques, D. A., Lucek, K., Meier, J. I., Mwaiko, S., Wagner, C. E., Excoffier, L., & Seehausen, O. (2016). Genomics of rapid incipient speciation in sympatric threespine stickleback. *PLoS Genetics*, *12*(2), e1005887. doi: 10.1371/journal.pgen.1005887

Martin, F. D., Cohen, A. E., Labay, B. J., Casarez, M. J., & Hendrickson, D. A. (2013). Apparent persistence of a landlocked population of Gulf pipefish, *Syngnathus scovelli*. *The Southwestern Naturalist*, *58*(3), 376–378. doi: 10.1894/0038-4909-58.3.376

Mattingsdal, M., Jorde, P. E., Knutsen, H., Jentoft, S., Stenseth, N. C., Sodeland, M., … Gonzalez, E. B. (2020). Demographic history has shaped the strongly differentiated corkwing wrasse populations in Northern Europe. *Molecular Ecology*, *29*(1), 160–171. doi: 10.1111/mec.15310

Mayr, E. (1947). Ecological Factors in Speciation. *Evolution*, *1*(4), 263–288. doi: 10.2307/2405327

McLane, W. M. (1955). *The Fishes of the St. Johns River System*.

Mérot, C., Oomen, R. A., Tigano, A., & Wellenreuther, M. (2020). A roadmap for understanding the evolutionary significance of structural genomic variation. *Trends in Ecology & Evolution*, *35*(7), 561–572. doi: 10.1016/j.tree.2020.03.002

Mobley, K. B., Small, C. M., Jue, N. K., & Jones, A. G. (2010). Population structure of the dusky pipefish (*Syngnathus floridae*) from the Atlantic and Gulf of Mexico, as revealed by mitochondrial DNA and microsatellite analyses. *Journal of Biogeography*, *37*(7), 1363–1377. doi: 10.1111/j.1365-2699.2010.02288.x

Muto, Y., & Okano, Y. (2010). CLERC and centrosomal leucine-rich repeat proteins. *Open Life Sciences*, *5*(1), 1–10. doi: 10.2478/s11535-009-0061-x

Noor, M. A. F., & Bennett, S. M. (2009). Islands of speciation or mirages in the desert? Examining the role of restricted recombination in maintaining species. *Heredity*, *103*(6), 439–444.

Nosil, P., Villoutreix, R., de Carvalho, C. F., Farkas, T. E., Soria-Carrasco, V., Feder, J. L., … Gompert, Z. (2018). Natural selection and the predictability of evolution in *Timema* stick insects. *Science*, *359*(6377), 765–770. doi: 10.1126/science.aap9125

Oksanen, J., Blanchet, F. G., Kindt, R., Legendre, P., Minchin, P. R., O'Hara, R. B., … Wagner, H. (2015). *vegan: Community Ecology Package*.

Partridge, C., Boettcher, A., & Jones, A. G. (2012). Population structure of the Gulf pipefish in and around Mobile Bay and the northern Gulf of Mexico. *Journal of Heredity*, *103*(6), 821–830. doi: 10.1093/jhered/ess062

Partridge, C., Cazalas, C., Rozelle, J., Hemming, J., & Boettcher, A. (2004). Small-scale captive breeding of a euryhaline pipefish. *World Aquaculture*, *35*, 51–54.

Partridge, C., Shardo, J., & Boettcher, A. (2007). Osmoregulatory role of the brood pouch in the euryhaline Gulf pipefish, *Syngnathus scovelli*. *Comparative Biochemistry and Physiology Part A: Molecular & Integrative Physiology*, *147*(2), 556–561. doi: http://dx.doi.org/10.1016/j.cbpa.2007.02.007

Peterson, B. K., Weber, J. N., Kay, E. H., Fisher, H. S., & Hoekstra, H. E. (2012). Double digest RADseq: An inexpensive method for de novo SNP discovery and genotyping in model and non-model species. *Plos One*, *7*(5), e37135.

Piazza, B. P., & La Peyre, M. K. (2009). The effect of Hurricane Katrina on nekton communities in the tidal freshwater marshes of Breton Sound, Louisiana, USA. *Estuarine, Coastal and Shelf Science*, *83*(1), 97–104. doi: 10.1016/j.ecss.2009.03.016

Pickrell, J. K., & Pritchard, J. K. (2012). Inference of population splits and mixtures from genome-wide allele frequency data. *PLoS Genetics*, *8*(11), e1002967. doi: 10.1371/journal.pgen.1002967

Portik, D. M., Leaché, A. D., Rivera, D., Barej, M. F., Burger, M., Hirschfeld, M., … Fujita, M. K. (2017). Evaluating mechanisms of diversification in a Guineo-Congolian tropical forest frog using demographic model selection. *Molecular Ecology*, *26*(19), 5245–5263. doi: 10.1111/mec.14266

Potts, W. T. W., & Hedges, A. J. (1991). Gill potentials in marine teleosts. *Journal of Comparative Physiology B*, *161*(4), 401–405. doi: 10.1007/BF00260800

Purcell, S., Neale, B., Todd-Brown, K., Thomas, L., Ferreira, M. A. R., Bender, D., … Sham, P. C. (2007). PLINK: a toolset for whole-genome association and population-based linkage analysis. *American Journal of Human Genetics*, *81*, 559–575.

Quast, W. D., & Howe, N. R. (1980). The osmotic role of the brood pouch in the pipefish *Syngnathus scovelli*. *Comparative Biochemistry and Physiology Part A: Physiology*, *67*(4), 675–678. doi: http://dx.doi.org/10.1016/0300-9629(80)90259-5

R Core Team. (2017). *R: A Language and Environment for Statistical Computing*. Vienna, Austria.

Rasband, W. S. (1997). *ImageJ*. U. S. National Institutes of Health, Bethesda, Maryland, USA.

Ravinet, M., Faria, R., Butlin, R. K., Galindo, J., Bierne, N., Rafajlović, M., … Westram, A. M. (2017). Interpreting the genomic landscape of speciation: A road map for finding barriers to gene flow. *Journal of Evolutionary Biology*, *30*(8), 1450–1477. doi: 10.1111/jeb.13047

Ravinet, M., Westram, A., Johannesson, K., Butlin, R., André, C., & Panova, M. (2015). Shared and non-shared genomic divergence in parallel ecotypes of *Littorina saxatilis* at a local scale. *Molecular Ecology*. doi: 10.1111/mec.13332

Renaut, S., Maillet, N., Normandeau, E., Sauvage, C., Derome, N., Rogers, S. M., & Bernatchez, L. (2012). Genome-wide patterns of divergence during speciation: The lake whitefish case study. *Philosophical Transactions of the Royal Society B: Biological Sciences*, *367*(1587), 354–363. doi: 10.1098/rstb.2011.0197

Rennison, D. J., Delmore, K. E., Samuk, K., Owens, G. L., & Miller, S. E. (2020). Shared patterns of genome-wide differentiation are more strongly predicted by geography than by ecology. *The American Naturalist*, *195*(2), 192–200. doi: 10.1086/706476

Riquet, F., Liautard-Haag, C., Woodall, L., Bouza, C., Louisy, P., Hamer, B., … Bierne, N. (2019). Parallel pattern of differentiation at a genomic island shared between clinal and mosaic hybrid zones in a complex of cryptic seahorse lineages. *Evolution*, *73*, 817–835. doi: 10.1111/evo.13696

Rohlf, F. J. (2005). *TpsDig2, digitize landmarks and outlines*. Department of Ecology and Evolution, State University of New York at Stony Brook.

Rose, E., Paczolt, K. A., & Jones, A. G. (2013). The contributions of premating and postmating selection episodes to total selection in sex-role-reversed Gulf pipefish. *The American Naturalist*, *182*(3), 410–420. doi: 10.1086/671233

Rougemont, Q., & Bernatchez, L. (2018). The demographic history of Atlantic salmon (*Salmo salar*) across its distribution range reconstructed from approximate Bayesian computations. *Evolution*, *72*(6), 1261–1277. doi: 10.1111/evo.13486

Rougemont, Q., Gagnaire, P.-A., Perrier, C., Genthon, C., Besnard, A.-L., Launey, S., & Evanno, G. (2017). Inferring the demographic history underlying parallel genomic divergence among pairs of parasitic and nonparasitic lamprey ecotypes. *Molecular Ecology*, *26*(1), 142–162. doi: 10.1111/mec.13664

Rougemont, Q., Moore, J.-S., Leroy, T., Normandeau, E., Rondeau, E. B., Withler, R. E., … Bernatchez, L. (2020). Demographic history shaped geographical patterns of deleterious mutation load in a broadly distributed Pacific Salmon. *PLOS Genetics*, *16*(8), e1008348. doi: 10.1371/journal.pgen.1008348

Rougeux, C., Bernatchez, L., & Gagnaire, P.-A. (2017). Modeling the multiple facets of speciation-with-gene-flow toward inferring the divergence history of lake whitefish species pairs (*Coregonus clupeaformis*). *Genome Biology and Evolution*, *9*(8), 2057–2074. doi: 10.1093/gbe/evx150

Roux, C., Fraïsse, C., Castric, V., Vekemans, X., Pogson, G. H., & Bierne, N. (2014). Can we continue to neglect genomic variation in introgression rates when inferring the history of speciation? A case study in a *Mytilus* hybrid zone. *Journal of Evolutionary Biology*, *27*(8), 1662–1675. doi: https://doi.org/10.1111/jeb.12425

Roux, C., Fraïsse, C., Romiguier, J., Anciaux, Y., Galtier, N., & Bierne, N. (2016). Shedding light on the grey zone of speciation along a continuum of genomic divergence. *PLOS Biology*, *14*(12), e2000234. doi: 10.1371/journal.pbio.2000234

Ruzicka, L., Howe, D., Ramachandran, S., Toro, S., Van Slyke, C., Bradford, Y., … Westerfield, M. (2019). The Zebrafish Information Network: New support for non-coding genes, richer Gene Ontology annotations and the Alliance of Genome Resources. *Nucleic Acids Research*, *47*(D1), D867–D873.

Schield, D. R., Adams, R. H., Card, D. C., Corbin, A. B., Jezkova, T., Hales, N. R., … Castoe, T. A. (2018). Cryptic genetic diversity, population structure, and gene flow in the Mojave rattlesnake (*Crotalus scutulatus*). *Molecular Phylogenetics and Evolution*, *127*, 669–681. doi: 10.1016/j.ympev.2018.06.013

Schluter, D., & Conte, G. L. (2009). Genetics and ecological speciation. *Proceedings of the National Academy of Sciences*, *106*(Supplement 1), 9955–9962. doi: 10.1073/pnas.0901264106

Serkov, V. M., Kornienko, M. S., & Kolobov, V. A. (2007). Structural and functional features of gill epithelium and the brood pouch of pipefish *Sygnathus acusimilis* (Syngnathidae, Gasterosteiformes) during adaptation to dilute sea water. *Journal of Ichthyology*, *47*(9), 750–754. doi: 10.1134/s0032945207090081

Small, C. M., Bassham, S., Catchen, J., Amores, A., Fuiten, A. M., Brown, R. S., … Cresko, W. A. (2016). The genome of the Gulf pipefish enables understanding of evolutionary innovations. *Genome Biology*, *17*(1), 258. doi: 10.1186/s13059-016-1126-6

Soria-Carrasco, V., Gompert, Z., Comeault, A. A., Farkas, T. E., Parchman, T. L., Johnston, J. S., … Nosil, P. (2014). Stick insect genomes reveal natural selection's role in parallel speciation. *Science*, *344*(6185), 738–742. doi: 10.1126/science.1252136

Stern, D. L. (2013). The genetic causes of convergent evolution. *Nature Reviews Genetics*, *14*(11), 751–764. doi: 10.1038/nrg3483

Sternberg, E. D., & Thomas, M. B. (2014). Local adaptation to temperature and the implications for vector-borne diseases. *Trends in Parasitology*, *30*(3), 115–122. doi: 10.1016/j.pt.2013.12.010

Storey, J. D., Bass, A., Dabney, A., & Robinson, D. (2019). qvalue: Q-value estimation for false discovery rate control (Version R package version 2.1.6.0). Retrieved from http://github.com/jdstorey/qvalue

Tenaillon, O., Rodríguez-Verdugo, A., Gaut, R. L., McDonald, P., Bennett, A. F., Long, A. D., & Gaut, B. S. (2012). The molecular diversity of adaptive convergence. *Science*, *335*(6067), 457–461. doi: 10.1126/science.1212986

Tine, M., Kuhl, H., Gagnaire, P.-A., Louro, B., Desmarais, E., Martins, R. S. T., … Reinhardt, R. (2014). European sea bass genome and its variation provide insights into adaptation to euryhalinity and speciation. *Nature Communications*, *5*, 5770. doi: 10.1038/ncomms6770

Via, S. (2001). Sympatric speciation in animals: The ugly duckling grows up. *Trends in Ecology & Evolution*, *16*(7), 381–390. doi: 10.1016/S0169-5347(01)02188-7

Wang, Y., Zhao, Y., Wang, Y., Li, Z., Guo, B., & Merilä, J. (2020). Population transcriptomics reveals weak parallel genetic basis in repeated marine and freshwater divergence in nine-spined sticklebacks. *Molecular Ecology*, *29*, 1642–1656. doi: 10.1111/mec.15435

Wellenreuther, M., & Bernatchez, L. (2018). Eco-evolutionary genomics of chromosomal inversions. *Trends in Ecology & Evolution*, *33*(6), 427–440. doi: 10.1016/j.tree.2018.04.002

Westram, A. M., Rafajlović, M., Chaube, P., Faria, R., Larsson, T., Panova, M., … Butlin, R. (2018). Clines on the seashore: The genomic architecture underlying rapid divergence in the face of gene flow. *Evolution Letters*, *2*(4), 297–309. doi: 10.1002/evl3.74

Whatley, E.C. (1962). Occurrence of breeding Gulf pipefish, *Syngnathus scovelli*, in the inland fresh waters of Louisiana. *Copeia*, *1962*(1), 220–220. doi: 10.2307/1439511

Whatley, E. C. (1969). A study of *Syngnathus scovelli* in fresh waters of Louisiana and salt waters of Mississippi. *Gulf and Caribbean Research*, *2*(4), 437–474. doi: 10.18785/grr.0204.02

White, M. J. D. (1968). Models of speciation. *Science*, *159*(3819), 1065–1070.

Wu, C.-I. (2001). The genic view of the process of speciation. *Journal of Evolutionary Biology*, *14*(6), 851–865. doi: 10.1046/j.1420-9101.2001.00335.x

Xue, A. T., & Hickerson, M. J. (2020). Comparative phylogeographic inference with genome-wide data from aggregated population pairs. *Evolution*, *74*(5), 808–830. doi: 10.1111/evo.13945

Table Captions

Table 1. Summary of data for each population. Shown are the surface water temperature (in °C), salinity (in parts per thousand), and index of seagrass density (scale of 0-5, with 0 being bare sand and 5 being densely covered with no bare patches), as measured at the time of sample collection. Also shown are the numbers of pregnant males, non-pregnant males, females, and juveniles retained in the analyses, with the total numbers sequenced included in parentheses. We also report the average observed heterozygosity (plus and minus the standard error of the mean), minor allele frequency (and the standard error of the mean), and percent polymorphic loci in each population. We report the values for the full dataset (7433 SNPs found in all 16 populations) alongside the numbers of individuals in the subsetted dataset (12103 SNPs found in 4 freshwater and 3 saltwater populations), with the subsetted dataset shown in parentheses. Note that these numbers are different because the filtering step using radiator (Gosselin, 2019) removed some individuals from the full dataset that were not removed from the subsetted dataset.

Table 2. The average pairwise F_{ST} values calculated from the full dataset by Stacks are shown in the upper triangle, color-coded in shades of blue where darker colors represent larger values, and thus greater differentiation. The largest pairwise F_{ST} is 0.254 between FLFW and TXFW. Along the diagonal are the variances estimated by Treemix, shaded from light grey to dark grey to help visualize which populations had larger variances (FLFW had the largest variance at 0.0216). In the lower diagonal we present the covariances calculated by Treemix, color-coded in shades of green where dark colors represent larger covariance magnitudes, and thus greater similarity. Both the Treemix variances and covariances are taken from a maximum likelihood tree estimated by Treemix without a root, with no migration edges, with blocks of 100 SNPs, and with the consensus tree as input.

Figure Captions

Figure 1. The collection locations of the marine populations (black circles) and the freshwater populations (blue diamonds) on a map of the southeastern USA (**A**). One migration event is supported in the treemix analysis, from the branch between FLAB (the root) and the other populations leading to FLPB. (**B**). The ADMIXTURE results for two runs with similarly low error rates, *K*=5 and *K*=7, reflect the pattern of isolation by distance described in Flanagan *et al.* (2016) and reflects the branching patterns in the treemix analysis (**C**). The PCAdapt analysis with *K*=7 clusters reveals that the first axis of variation explains differences between the east coast of Florida and the rest of the populations and the second axis of variation separates the Florida freshwater population from the others, and the next two axes split apart populations by geographic location and freshwater or saltwater status (**D**).

Figure 2. The best-fitting $\delta_A\delta_I$ models for each freshwater population and its nearest saltwater neighbor. Shown for each pair are the two-dimensional joint frequency spectrum for the data versus the model along with the residuals for each model. To the right of those four plots are schematics for the best fitting model. Counterclockwise from top left, the comparisons are: FLFW vs. FLCC (best model: isolation with migration); ALFW vs. ALST (best model: secondary contact with heterogeneous migration rates genome-wide and changes in population size); LAFW vs. ALST (best model: secondary contact with heterogeneous migration rates genome-wide and changes in population size); TXFW vs. TXCC (best model: isolation with migration with heterogeneous migration rates genome-wide). For more information see Supplement 2.

Figure 3. In (**A**) are the pairwise AMOVA-corrected F_{ST} values for each freshwater-marine comparison calculated by Stacks. The top panel shows the Texas comparison, the second the Alabama comparison, the third the Louisiana comparison, and the bottom panel shows the Florida comparison. In each panel the alternating colors represent different chromosomes, which are numbered along the x-axis. The 50 SNPs that were outliers in all Stacks F_{ST} comparisons (except Florida) are marked with pink asterisks and the SNPs that were significant in all three permutation analyses are marked with red diamonds. Note that some outliers are not pictured as they are on unanchored scaffolds. The upset plot in (**B**) shows the overlap among the four pairwise Stacks F_{ST} comparisons, highlighting that 7 SNPs are outliers in all four comparisons, but that most overlap occurs between Louisiana, Alabama,

and Texas. The upset plot in **(C)** shows similar patterns for the permutations, and also identifies the overlap between the permutation analyses and the outliers shared in the pairwise Louisiana, Alabama, and Texas Stacks analysis ('Stacks' does not include Florida).

Figure 4. In **(A)**, the genome-wide distribution of Bayenv $X^{T}X$ values (top panel of A) and the logarithm of the Bayes Factors associated with salinity in Bayenv (bottom panel of A) are shown. Alternating light and grey points represent the chromosomes, which are numbered along the x-axis. Bayenv $X^{T}X$ outliers are marked with an orange +; and salinity-correlated outliers are marked with a blue triangle. In **(B)**, the overlap in outliers among analyses is shown in an upset plot.

Population	Temperature	Salinity	Seagrass Density	N_Pregnant	N_NonPregnant	N_Female	N_Juvenile	Observed heterozygosity	Minor Allele Frequency	Percent Polymorphic Loci
ALFW	31	0	3	21 (23)	3 (4)	13 (21)	0 (0)	0.026±0.006 (0.021±0.007)	0.017±0.004 (0.012±0.003)	30 (28.2)
ALST	28.5	25	2	20 (24)	0 (0)	23 (23)	0 (0)	0.041±0.008 (0.031±0.009)	0.024±0.004 (0.017±0.003)	46.1 (42.1)
FLAB	33	36	4	4 (5)	13 (18)	17 (19)	0 (0)	0.057±0.012 (0.026±0.01)	0.037±0.007 (0.445±0.235)	44.6 (60.8)
FLCC	33	21	3	2 (7)	9 (12)	16 (18)	4 (4)	0.037±0.011 (0.023±0.01)	0.036±0.016 (0.02±0.009)	18.7 (15.2)
FLFD	33	21	4	19 (22)	0 (0)	16 (18)	0 (0)	0.046±0.008 (0.024±0.008)	0.03±0.005 (0.444±0.235)	47.1 (62.3)
FLHB	32	25	3	11 (11)	2 (2)	20 (20)	8 (8)	0.043±0.014 (0.024±0.011)	0.038±0.016 (0.448±0.237)	23.1 (53.3)
FLKB	30.5	20	2	21 (21)	0 (0)	19 (21)	0 (0)	0.056±0.01 (0.029±0.01)	0.034±0.005 (0.446±0.234)	56.2 (65.8)
FLFW	30	0	4	0 (0)	3 (3)	16 (17)	23 (27)	0.014±0.007 (0.013±0.008)	0.038±0.03 (0.021±0.016)	6.7 (5.2)
FLPB	30	20	3	18 (18)	1 (1)	9 (10)	14 (14)	0.043±0.013 (0.024±0.011)	0.037±0.014 (0.447±0.237)	25.5 (54.1)
FLSG	30.5	26	3	20 (20)	0 (0)	21 (21)	2 (3)	0.054±0.009	0.033±0.005	55.4 (65.7)

								(0.028±0.01)	(0.446±0.234)	
FLSI	30	30	4	22 (23)	0 (0)	18 (22)	0 (0)	0.053±0.01 (0.027±0.009)	0.033±0.005 (0.445±0.235)	52.3 (64)
LAFW	28	0	3	23 (25)	9 (10)	4 (9)	3 (4)	0.031±0.007 (0.023±0.008)	0.02±0.004 (0.014±0.003)	34.8 (32.2)
TXCB	28	35	2	18 (21)	1 (1)	11 (14)	0 (0)	0.037±0.009 (0.025±0.01)	0.025±0.007 (0.445±0.236)	28.9 (58.9)
TXCC	33	48	2	14 (15)	2 (2)	15 (19)	5 (5)	0.038±0.008 (0.031±0.01)	0.026±0.006 (0.019±0.005)	33.2 (27.9)
TXFW	31	0	2	1 (1)	2 (4)	5 (5)	19 (21)	0.032±0.011 (0.023±0.011)	0.026±0.01 (0.017±0.007)	13.5 (8.9)
TXSP	29	32	3	31 (39)	0 (0)	12 (20)	2 (3)	0.036±0.008 (0.026±0.01)	0.024±0.006 (0.445±0.235)	33.3 (62.8)

Table 2.

	TXSP	TXCC	TXFW	TXCB	LAFW	ALST	ALFW	FLSG	FLKB	FLFD	FLSI	FLAB	FLPB	FLHB	FLCC	FLFW
TXSP	0.0042	0.007	0.0378	0.0148	0.0251	0.0224	0.0243	0.0287	0.0296	0.0318	0.0312	0.0398	0.0627	0.0673	0.0719	0.1175
TXCC	0.0041	0.0041	0.0386	0.014	0.0259	0.0225	0.0258	0.0283	0.0292	0.0317	0.0309	0.0392	0.0628	0.0677	0.0725	0.1208
TXFW	0.003	0.0031	0.0078	0.0422	0.0425	0.0368	0.0437	0.0396	0.0404	0.0466	0.0434	0.0559	0.0977	0.1074	0.124	0.254
TXCB	0.0037	0.0038	0.0033	0.0043	0.0275	0.0233	0.028	0.0288	0.0297	0.0331	0.0317	0.0405	0.0665	0.0721	0.0787	0.1368
LAFW	0.0011	0.0011	0.0013	0.0012	0.0028	0.0109	0.012	0.0212	0.0223	0.0252	0.0245	0.0333	0.0533	0.0579	0.062	0.1052

ALST	0.0011	0.0011	0.0008	0.0011	0.0019	0.0022	0.0138	0.0171	0.0182	0.0203	0.0204	0.028	0.0461	0.0495	0.0514	0.0841
ALFW	0.0014	0.0013	0.0018	0.0014	0.0023	0.0017	0.0029	0.0216	0.0229	0.0262	0.0251	0.0345	0.0563	0.0611	0.0671	0.1166
FLSG	-0.0004	-0.0004	-0.0006	-0.0004	0.0003	0.0006	0.0003	0.0021	0.0074	0.0126	0.0126	0.0207	0.0405	0.0435	0.044	0.0728
FLKB	-0.0005	-0.0005	-0.0007	-0.0005	0.0002	0.0005	0.0001	0.002	0.0022	0.0115	0.0115	0.0202	0.0406	0.0437	0.0442	0.0734
FLFD	-0.0004	-0.0004	-0.0007	-0.0005	0.0001	0.0003	0	0.0015	0.0017	0.0023	0.008	0.0201	0.044	0.0477	0.0496	0.085
FLSI	-0.0006	-0.0006	-0.0009	-0.0006	0	0.0003	-0.0001	0.0016	0.0017	0.0023	0.0026	0.0185	0.0424	0.0458	0.0466	0.0776
FLAB	-0.0011	-0.0011	-0.0014	-0.0011	-0.0006	-0.0002	-0.0006	0.001	0.0011	0.0014	0.0017	0.0037	0.0454	0.0503	0.0515	0.0913
FLPB	-0.0036	-0.0036	-0.0038	-0.0035	-0.0027	-0.0025	-0.0028	-0.0016	-0.0015	-0.0015	-0.0015	-0.0002	0.0073	0.0074	0.0094	0.0982
FLHB	-0.0038	-0.0038	-0.004	-0.0037	-0.0029	-0.0027	-0.003	-0.0018	-0.0017	-0.0017	-0.0017	-0.0005	0.0078	0.0085	0.0078	0.1067
FLCC	-0.0037	-0.0038	-0.004	-0.0037	-0.0028	-0.0027	-0.003	-0.0018	-0.0017	-0.0017	-0.0017	-0.0006	0.0078	0.0085	0.0085	0.1336
FLFW	-0.0045	-0.0045	-0.005	-0.0045	-0.0036	-0.0036	-0.0038	-0.0026	-0.0026	-0.0025	-0.0024	-0.0013	0.0058	0.0064	0.0066	0.0223

Supplementary Figure and Caption Legends

Supplement 1

Figure S1.1. Principal components analysis of morphological traits in *S. scovelli* reveals that phenotypic variation among populations is not based on habitat type. The top set of panels show the results of the PCA with all 16 populations, color-coded by populations and point shape. The bottom set of panels show the same PCA results, but with different x- and y-axis scaling and without the saltwater populations plotted, to facilitate visualizing the differences among saltwater populations. The left panels show male body traits (SVL, tail length, trunk depth, head length, snout length, and snout depth), the middle panels show those same traits in females, and the right panels show the female band traits (band number and band area).

Figure S1.2. Minor allele frequency distributions of the full dataset (7433 SNPs) for each population. Freshwater populations are plotted in blue. The histograms show the number of SNPs with various frequencies of the reference alleles. All populations are skewed towards having small minor allele frequencies, but the TXFW and FLFW have additional reductions in genetic variation.

Figure S1.3. Heatmaps depicting population structure. In all graphs, dark colors depict similarity between populations and light grey and blue depict populations with high differentiation. The left panel shows pairwise FST values calculated by the populations module in Stacks (Catchen et al. 2013). The right panel shows covariances between populations as calculated by TreeMix (Pickrell and Pritchard 2012).

Figure S1.4. Scree plot from PCAdapt, specifying keeping 20 PC axes.

Figure S1.5. Principal components analysis of genotypes in *S. scovelli* reveals population structure due to geographic distance and habitat type. The top set of panels show the results of the PCA with all 16 populations, color-coded by populations and point shape. The bottom set of panels show the same PCA results, but with different x- and y-axis scaling and without the saltwater populations plotted, to facilitate visualizing the differences among saltwater populations. The left panels show the first and second PC axes, which together account for 53.5% of the variation, the middle panels show the 3rd and 4th PC axes (another 26.8% of the variation), and the right panels the fifth and sixth axes (another % of variation).

Figure S1.6. Admixture screeplot for K=1 through K=16. The coefficient of variation (CV) is shown on the y-axis.

Figure S1.7. Admixture plot for K=2. The colors represent different genetic populations.

Figure S1.8. Admixture plot for K=3. The colors represent different genetic populations.

Figure S1.9. Admixture plot for K=4. The colors represent different genetic populations.

Figure S1.10. Admixture plot for K=5. The colors represent different genetic populations.

Figure S1.11. Admixture plot for K=6. The colors represent different genetic populations.

Figure S1.12. Admixture plot for K=7. The colors represent different genetic populations.

Figure S1.13. The consensus tree from running Treemix without any migration edges and no root.

Figure S1.14. The consensus tree from running Treemix without any migration edges and FLAB as root.

Figure S1.15. Plot showing the comparison of Treemix number of migration edges using the Evanno method.

Figure S1.16. Average log likelihoods of treemix bootstrap replicates with 0 through 5 migration edges. Shown are the means (of 100 bootstraps) and the standard error of the mean.

Figure S1.17. The plot of the tree with FLAB as root but no migration edges (left) compared to the tree with FLAB as root and two migration edges. The drift parameter is plotted on the x-axis, and migration edges are colored based on the migration weight.

Figure S1.18. Plot of the f3 statistic for three-population trees including both FLPB and FLAB. Error bars show the standard errors generated from block jackknifes. Trees indicative of admixture in FLPB are those with significantly negative f3 statistics.

Figure S1.19. Plot of the f4 statistic for four-population trees including both FLPB and FLAB and other Florida populations. Error bars show the standard errors generated from block jackknifes. Trees indicative of admixture in the tree are those with significantly non-zero f4 statistics.

Table S1.1. Proportion of variation explained by all 7 of the retained PC axes in PCAdapt.

Table S1.2. Number of bootstraps with the one migration edge beginning at each of these points on the population trees.

Table S1.3. Number of bootstraps with the one migration edge ending at each of these points on the population trees.

Table S1.4. Four-population trees with FLPB and FLAB and their f4 statistic, standard error, z-score, and p-value.

Supplement 2

Figure S2.1. Schematic diagrams of each model, color-coded by base model (Strict Isolation, Isolation with Migration, Ancient Migration, or Secondary Contact). 'Linked Sel.' refers to linked selection, where a sub-section of the genome experienced a different effective population size than the remainder of the genome (hrf). 'Het. Migration' refers to differential introgression, where some regions of the genome experienced different migration rates than others. Each row demonstrates how parameters were added to the base models. Strict Isolation models contained now migration, so only linked selection and growth could be incorporated. Under Isolation with Migration scenarios, differentiating between linked selection and heterogeneous migration is difficult, so the models that combined both were not included for the Isolation with Migration scenarios.

Figure S2.2. Comparison of log likelihoods for FLFW-FLCC models.

Figure S2.3. Boxplot showing the parameter estimates from the replicates of the SI model (left) and the IM model (right) for the FLFW vs FLCC pairwise comparison. The red stars represent the model parameters from the run with the highest log likelihood.

Figure S2.4. Comparison of log likelihoods for FLFW-FLCC models.

Figure S2.5. Summary plot of the joint site frequency spectrum of the data for the FLFW vs FLCC comparison (left) and the best-fitting model (right), plus their residuals (bottom row).

Figure S2.6. Comparison of log likelihoods for the simple ALFW-ALST models.

Figure S2.7. Comparison of log likelihoods for the complex IM models for ALFW-ALST.

Figure S2.8. Comparison of log likelihoods for the complex SC models for ALFW-ALST.

Figure S2.9. Summary plot of the joint site frequency spectrum of the data for the ALFW vs ALST comparison (left) and the best-fitting model (right), plus their residuals (bottom row).

Figure S2.10. Comparison of log likelihoods for ALST-LAFW models.

Figure S2.11. Comparison of log likelihoods for ALST-LAFW models.

Figure S2.12. Summary plot of the joint site frequency spectrum of the data for the ALST vs LAFW comparison (left) and the best-fitting model (right), plus their residuals (bottom row).

Figure S2.13. Comparison of log likelihoods for TXFW-TXCC models.

Figure S2.14. Comparison of log likelihoods for TXFW-TXCC models.

Figure S2.15. Summary plot of the joint site frequency spectrum of the data for the TXFW vs TXCC comparison (left) and the best-fitting model (right), plus their residuals (bottom row).

Table S2.1. For each analysis of the freshwater-saltwater pairs, the retained number of individuals (the values in this table were multiplied by 2 for the projections used in dadi) in each population and the number of SNPs retained in each analysis.

Table S2.2. Table describing all of the parameters from the dadi models and which models they appear in.

Table S2.3. Table showing the results of the run with the median log likelihood for each model for the FLFW vs FLCC comparison. The parameters are not converted to biologically realistic values, and their meanings are presented in Table S2.2.

Table S2.4. Table showing the results of the run with the median log likelihood for each model for the FLFW vs FLCC comparison. The parameters are not converted to biologically realistic values, and their meanings are presented in Table S2.2.

Table S2.5. Table showing the results of the run with the median log likelihood for each model for the ALFW vs ALST comparison. The parameters are not converted to biologically realistic values, and their meanings are presented in Table S2.2.

Table S2.6. Table showing the results of the run with the median log likelihood for each model for the ALFW vs ALST comparison. The parameters are not converted to biologically realistic values, and their meanings are presented in Table S2.2.

Table S2.7. Table showing the results of the run with the median log likelihood for each model for the ALST vs LAFW comparison. The parameters are not converted to biologically realistic values, and their meanings are presented in Table S2.2.

Table S2.8. Table showing the results of the run with the median log likelihood for each model for the ALST vs LAFW comparison. The parameters are not converted to biologically realistic values, and their meanings are presented in Table S2.2.

Table S2.9. Table showing the results of the run with the median log likelihood for each model for the TXFW vs TXCC comparison. The parameters are not converted to biologically realistic values, and their meanings are presented in Table S2.2.

Table S2.10. Table showing the results of the run with the median log likelihood for each model for the TXFW vs TXCC comparison. The parameters are not converted to biologically realistic values, and their meanings are presented in Table S2.2.

Table S2.11. Table of all of the parameters for the best models for each population pair.

Supplement 3

Figure S3.1. Manhattan plot of pairwise AMOVA-corrected Fst values from Stacks for each freshwater - nearest saltwater population pair. The x-axis corresponds to genomic locations, with chromosomes labelled. To the right are loci that mapped to unanchored scaffolds.

Figure S3.2. Manhattan plot of pairwise AMOVA-corrected Fst values from Stacks for the saltwater populations nearest to freshwater populations compared to their nearest saltwater neighbor. The x-axis corresponds to genomic locations, with chromosomes labelled. To the right are loci that mapped to unanchored scaffolds.

Figure S3.3. Distributions of the Stacks AMOVA-Corrected Fst values for the pairwise comparisons of each freshwater population and its nearest saltwater neighbor (main plots) and the pairwise comparisons of those saltwater populations and their nearset saltwater population (insets).

Figure S3.4. Upset plot with shared Stacks outliers identified using a cutoff of p=0.01. 'sharedStacks' refers to outliers shared in the Alabama, Louisiana, and Texas pairwise Fst comparisons from Stacks (at 0.01 threshold).

Figure S3.5. Upset plot with shared Stacks outliers shared with other outlier analyses (which are described below) identified using a cutoff of p=0.01. 'pcadapt' refers to the outliers identified using principal components analysis, 'permutations' refers to outliers from a permuted Fst distribution, 'sharedStacks' are those shared in the Alabama, Louisiana, and Texas pairwise Fst comparisons from Stacks (at 0.01 threshold), 'xtx' refers to the population-structure-corrected Fst analog calculated by Bayenv2, and 'salBF' are loci that are significantly correlated with salinity measurements (from Bayenv2).

Figure S3.6. Manhattan plot of pairwise Fst values. Data are the same as Figure 3 in the main text but the outliers plotted are the shared Stacks outliers with a threshold of 0.01 instead of 0.05.

Figure S3.7. Histograms of pairwise Fst values generated by the permutations (in grey) and the actual Fst values (in color in insets). Only loci with Fst values larger than zero are shown in the histograms.

Figure S3.8. Manhattan plot of pairwise average Fst values from the permutation of population IDs for each freshwater - nearest saltwater population pair. The x-axis corresponds to genomic locations, with chromosomes labelled. To the right are loci that mapped to unanchored scaffolds.

Figure S3.9. Manhattan plot of pairwise Fst values calculated for each freshwater - nearest saltwater population pair. The x-axis corresponds to genomic locations, with chromosomes labelled. To the right are loci that mapped to unanchored scaffolds.

Figure S3.10. Screeplot for the subsetted dataset with 20 PC axes retained in the analysis.

Figure S3.11. Plot of the scores from the PCAdapt outlier analysis with the subsetted dataset and 4 PC axes retained in the analysis.

Figure S3.12. Plots of the loadings for the four PC axes according to genomic position (on the x-axis).

Figure S3.13. Inspecting the loadings for the four PC axes according to genomic position (on the x-axis) for each chromosome individually.

Figure S3.14. Manhattan plot for the PCAdapt outlier analysis with the subsetted dataset and 4 PC axes retained in the analysis.

Figure S3.15. Q-Q plot for the PCAdapt outlier analysis with the subsetted dataset and 4 PC axes retained in the analysis.

Figure S3.16. Distribution of the for the PCAdapt outlier analysis with the subsetted dataset and 4 PC axes retained in the analysis. Figure S3.14. Manhattan plot of the PCAdapt statistics with the outliers from other analyses included.

Figure S3.17. Manhattan plot of the PCAdapt statistics with the outliers from other analyses included.

Figure S3.18. Heatmap plots of each of the ten replicate Bayenv covariance matrices. Darker colors represent higher covariances. Populations are in the order: ALFW, ALST, FLCC, FLFW, LAFW, TXCC, TXFW.

Figure S3.19. Manhattan plots of the Bayenv XTX statistic and the log of the Bayes factors associated with salinity. Shown are only loci that mapped to regions on chromosomes. Grey points represent loci that are not outlier in any analyses. Colored points represent outliers in both the Bayenv analyses and the other outlier analyses.

Figure S3.20. Upset plot showing overlap between the Bayenv analysis with Florida in it and the other analyses.

Figure S3.21. Plot of the outliers in their positions in LG6. Gene regions are shown in grey, the salinity-associated outliers are shown in the blue dashed lines, and the shared Stacks outliers (TX, AL, and LA only) are shown as pink lines. Outliers in gene regions have their gene abbreviation printed above the lines.

Figure S3.22. Heatmap plots of each of the ten replicate Bayenv covariance matrices when Florida was excluded from the analysis. Darker colors represent higher covariances. Populations are in the order: ALFW, ALST, LAFW, TXCC, TXFW.

Figure S3.23. Manhattan plots of the Bayenv XTX statistic and the log of the Bayes factors associated with salinity from the analysis without the Florida populations. Shown are only loci that mapped to regions on chromosomes. Grey points represent loci that are not outlier in any analyses. Colored points represent outliers in both the Bayenv analyses and the other outlier analyses.

Figure S3.24. Plots of the Bayenv statistics in the analysis with the Florida populations (x-axis) vs without the Florida populations (y-axis).

Figure S3.25. Plot of the outliers in their positions in LG6. Gene regions are shown in grey, the salinity-associated outliers are shown in the blue dashed lines, and the shared Stacks outliers (TX, AL, and LA only) are shown as pink lines. Outliers in gene regions have their gene abbreviation printed above the lines.

Table S3.1. The number of SNPs in each pairwise Fst comparisons in Stacks.

Table S3.2. Table summarizing the number of outliers found in the Stacks analysis when the significance threshold is set to 0.01 versus 0.05.

Table S3.3. Summary of the permutations. Presented are the mean and standard error of the mean for the actual and permuted Fst values for each comparison. Also shown are the number of outliers identified in each analysis, where outliers were defined as those loci whose actual Fst values we either larger or smaller than the maximum or minimum permuted Fst value.

Table S3.4. SNPs that were Fst outliers in all pairwise Texas, Alabama, and Louisiana Stacks and permutation analyses. Shown are the SNP ID in this dataset, the ID of the gene it is mapped to in the *S. scovelli* genome, its location and reference and alternative alleles. The final two columns show the type of genomic region the SNP is in and the gene description (if relevant).

Table S3.5. Number of outliers associated with each of the four retained principal components axes.

Table S3.6. Outliers on LG6 that were shared among Stacks Texas, Alabama, and Louisiana freshwater-saltwater pairwise AMOVA-corrected Fst analyses and also outliers in the salinity-association analysis from Bayenv2 WITH Florida, and any other analyses they were outliers in.

Table S3.7. Correlations between the Bayenv analyses without the Florida populations ('noFL') and with the Florida populations ('FL'). The comparison of each statistic with itself in each analysis is on the diagonal.

Table S3.8. Table summarizing the outliers from each analysis.

Table S3.9. The number of SNPs in the subsetted dataset that were outliers in coding and non-coding regions of the genome.

Table S3.10. The number of SNPs in the subsetted dataset that were outliers in putative salinity genes or not.

Table S3.11. Outliers on LG6 that were shared among Stacks Texas, Alabama, and Louisiana freshwater-saltwater pairwise AMOVA-corrected Fst analyses and also outliers in the salinity-association analysis from Bayenv2, and any other analyses they were outliers in.

Table S3.12. Table of putative freshwater adaptation genes and their gene ID name in the Gulf pipefish genome.